A unified PFEM formulation to simulate melt pool dynamics and its instabilities in metal additive manufacturing.

FRIA call 2020
Last updated on Monday 14th December, 2020

Simon FÉVRIER

Advisors:
Jean-Philippe PONTHOT, Romain BOMAN

LIÈGE université
Sciences Appliquées

Industrial context

Modelling of metal additive manufacturing

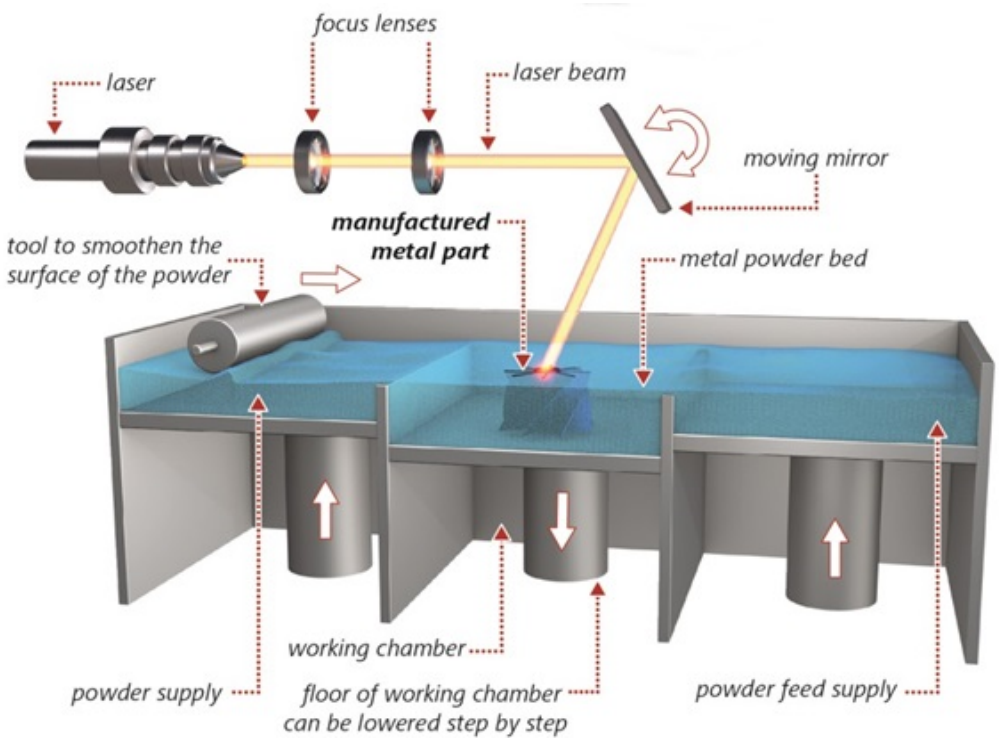

Selective Laser Melting concept, from `https://www.empa.ch/documents/147354/601833/SLM-Scheme2_570px.jpg/`.

Manufacture 3D parts with more flexibility than conventional methods $\rightarrow$ great industrial interest to improve performance:

- laser scanning speed,
- laser power.

How to improve performance without decreasing the quality ?

Underlying physics - mesoscopic scale

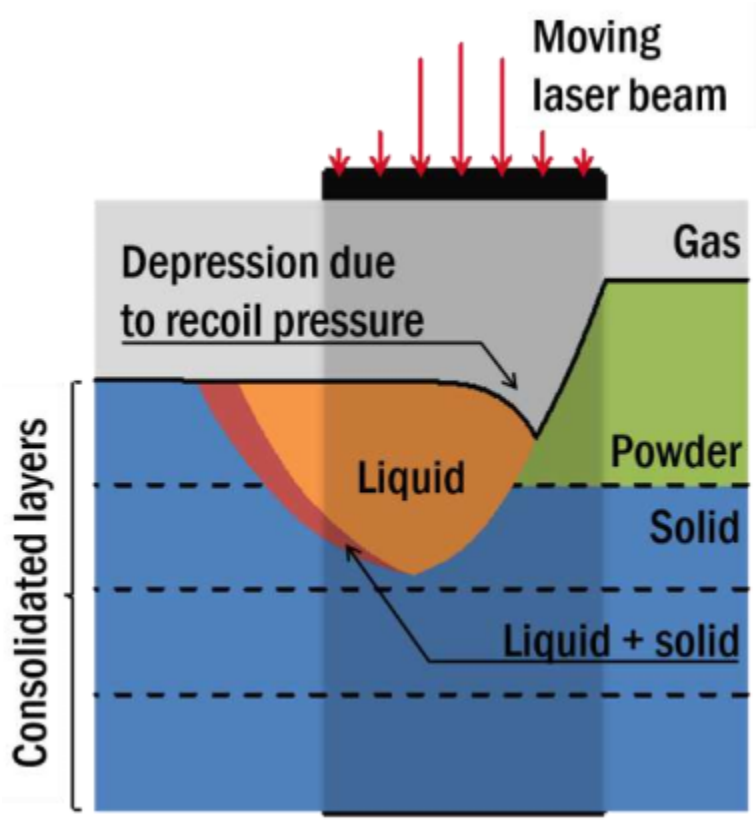

Melt pool dynamics. Adapted from Chen 2018.

Physics involved:

- Marangoni forces,
- Thermo-solid/fluid/gas coupling (geometrical distortions, residual stresses, recoil pressure ...),
- Phase changes and liquid dynamics,
- Laser interactions,
- etc.

Evolving melt pool frontier and upper surface unknown *a priori* $\rightarrow$ numerical challenge.

Detrimental effects

Multiple sources of defects: balling effect, spattering, etc.

In this project, study **Keyhole instabilities**: keyhole's wall collapses → gas trapped → pore.

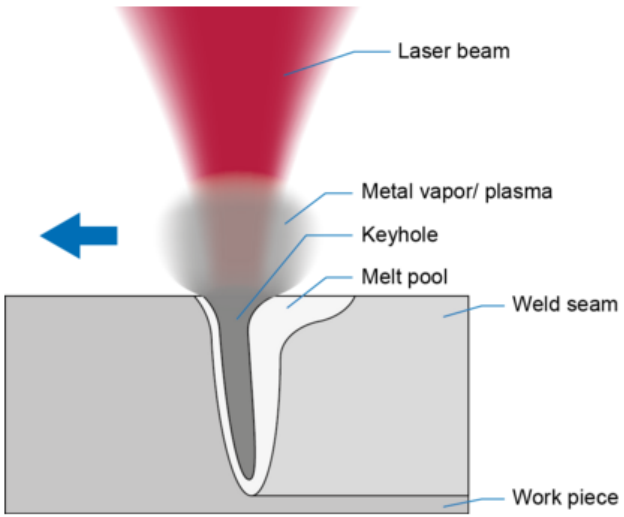

High laser power → keyhole. Adapted from Caprio 2020.

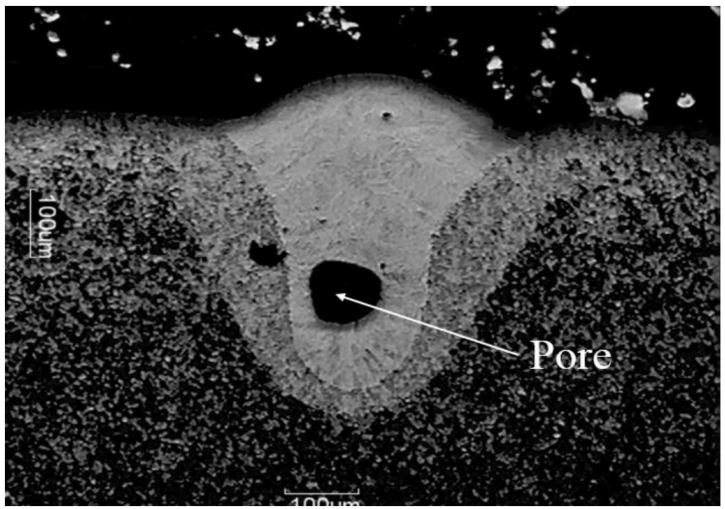

Porosities after keyhole collapse. From Kusuma 2016.

⇒ **porosities → quality of the manufactured part decreases.**

Detrimental effects

Front view orthogonal to scanning direction:

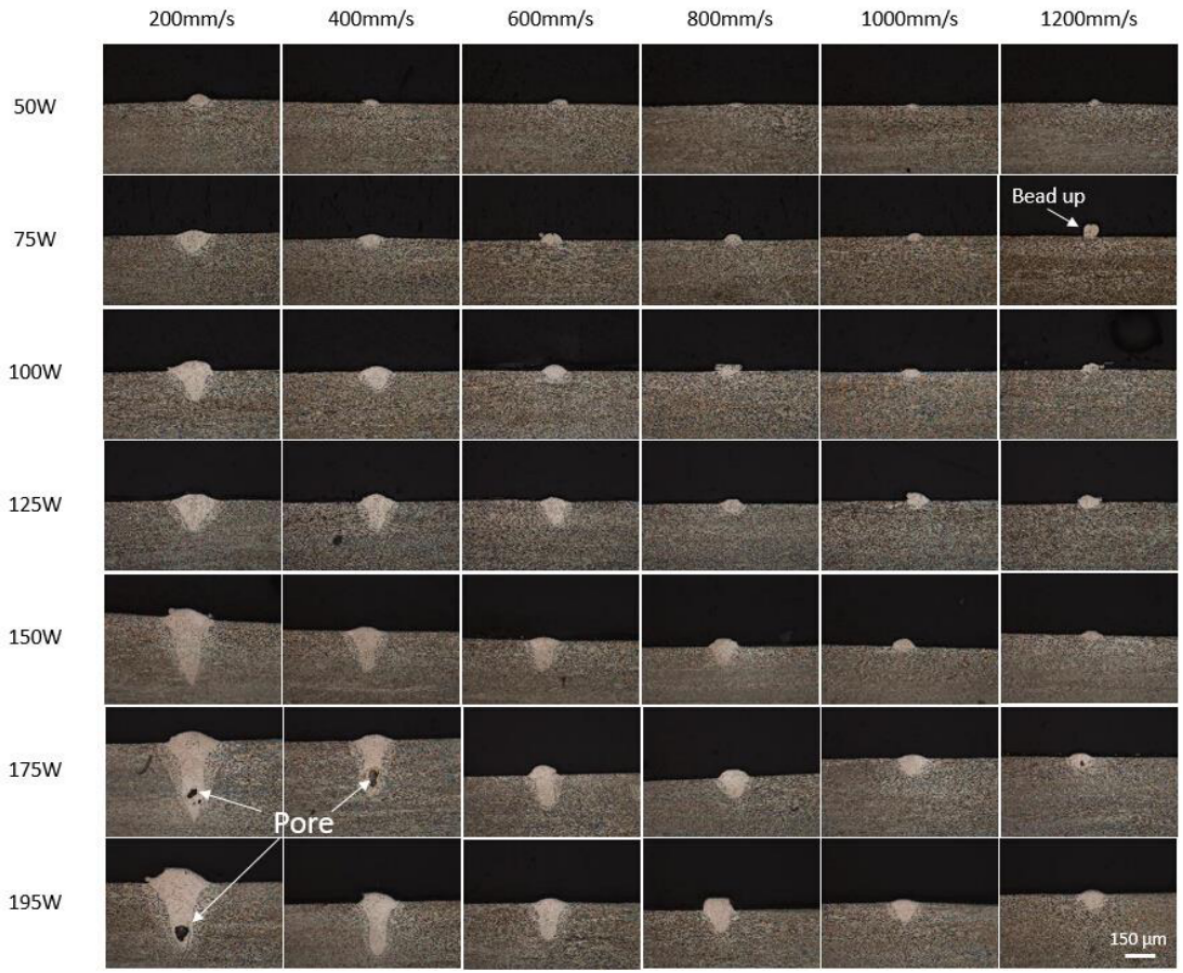

Melt pool profile of single beads (powder case, Ti-6Al-4V); from Gong 2014.

Goal of the research

Understand **melt pool dynamics** and **instabilities** at the mesoscopic scale, notably **deep keyholes** :

- Keyhole wall unstable ?
- Fluid flow inside the melt pool $\rightarrow$ aforementioned physical effects ?
- Effect of vaporized material (recoil pressure)?

Experiments difficult at these time scales, space scales and elevated temperature.

$\Rightarrow$ **3D computational model**, based on the **Particle Finite Element Method**, to study the physics of the melt pool.

State of the art

Most advanced models

In the literature, **Eulerian** methods (FEM or FVM, **mesh fixed in space**), with interface tracking algorithm (Volume of Fluid or Level-Set) and adaptive mesh refinement.

Example model: Quiang Chen PhD Thesis (2018, CEMEF, Sophia-Antipolis, advisor: M. Bellet).

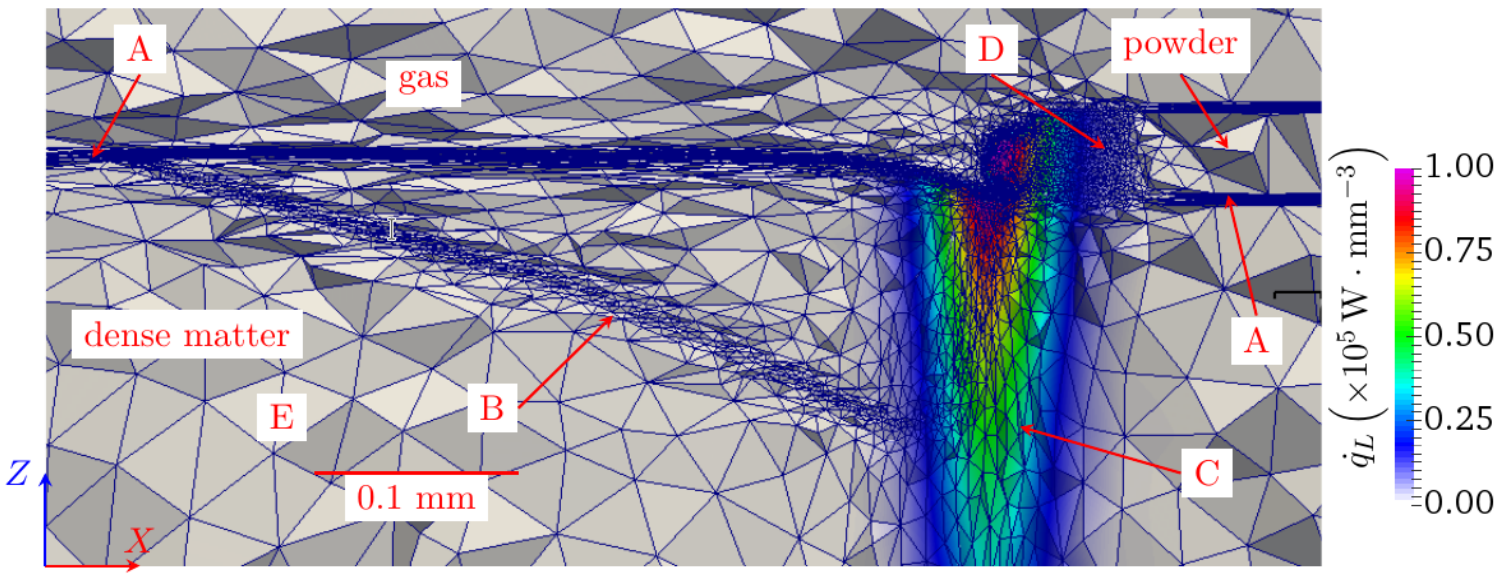

Example of mesh and heat source distribution from Chen, who uses Eulerian FEM, Level-Set and adaptive remeshing (essential ingredients).

Comments

Limitations of state of the art method (Eulerian, level-set, adaptive remeshing):

- complex implementation,
- accuracy of interface tracking limited,
- surrounding gas has to be discretized,
- no **spattering**, no powder **vaporisation**, no **keyhole instabilities**,
- limited to full fluid dynamics approach (no **residual stresses**).

$\Rightarrow$ Proposed approach based on the **Particle Finite Element Method**.

Proposed approach - The Particle Finite Element Method (PFEM)

The Particle Finite Element Method

Lagrangian method (mesh attached to material) based on the FEM:

1. material discretized as **cloud of nodes**, informations stored at node level,
2. mesh generated from the cloud of nodes (Delaunay triangulation and alpha-shape to automatically extract external boundaries),

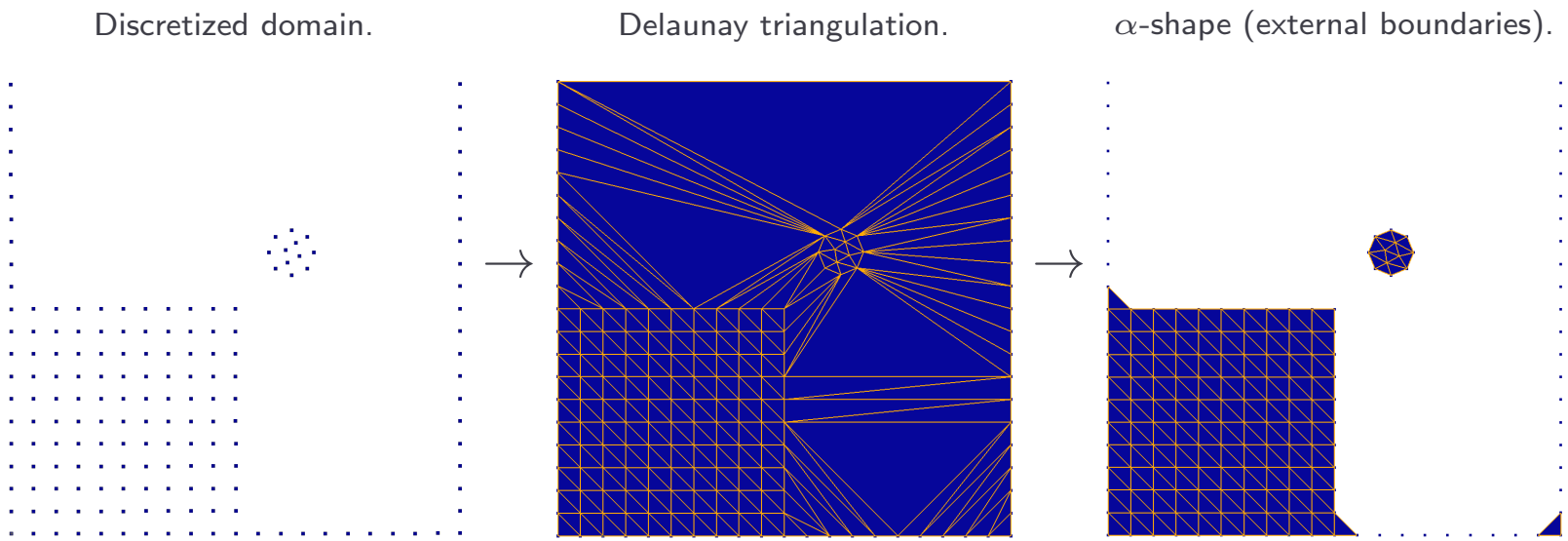

Delaunay triangulation (convex hull) and alpha-shape algorithm ($\rightarrow$ external boundaries), from Février's master thesis.

The Particle Finite Element Method - cont'd

3. FEM computations performed over one time step and then nodal informations updated,
4. remeshing procedure to ensure good mesh quality (avoid elements distortion).
5. Go to 1 for next time step.

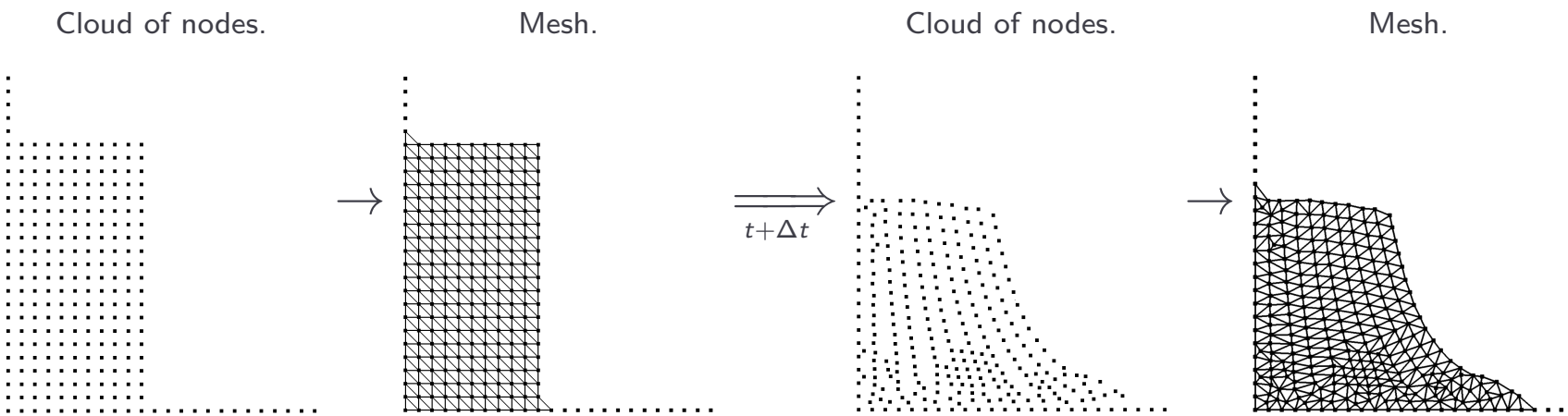

Dam Break: collapsing of a water column submitted to gravity, example of mesh update between two time steps.

Comments

Advantages of the proposed approach:

- relatively easy implementation
- informations stored at nodes $\rightarrow$ no interpolation of data after remeshing ($\rightarrow$ no diffusion),
- only the material of interest is discretized (surrounding gas not simulated),
- interface naturally tracked by the method (**Lagrangian** approach) ($\leftrightarrow$ level-set and adaptive mesh),
- **spattering** and **keyholes** can be modelled,
- solid mechanics can be introduced (and thus **residual stresses**).

Challenges

Numerical challenges:

- 3D implementation of a multiphysics problem with evolving boundaries,
- thermo-mechanical effects and phase changes,
- high-performance scientific computing.

Validation:

- comparison with results from the literature and other projects at ULiège,
- collaboration with other teams working on the problem (stay at CEMEF at Sophia Antipolis, Pr. Michel Bellet),
- collaboration with Pr. Anne Mertens and Anne-Marie Habraken at ULiège (SLM experiments).

Personal experience

Master Thesis

Engineering physics master thesis: first prototype of **3D** Newtonian flow solver using PFEM (from scratch, no thermal effect).

Poiseuille flow in pipe

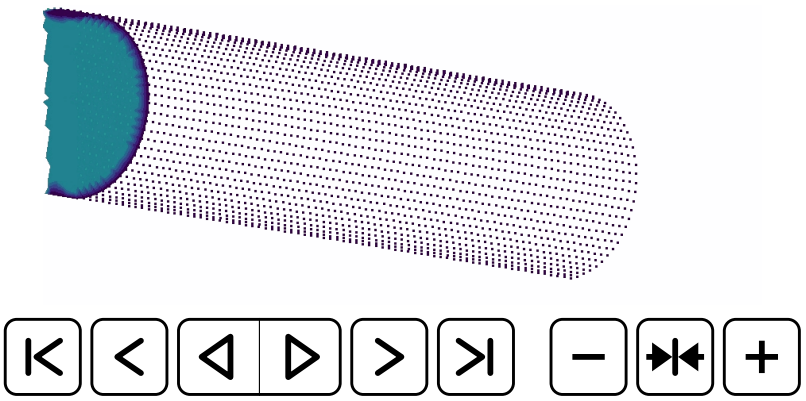

Dam break

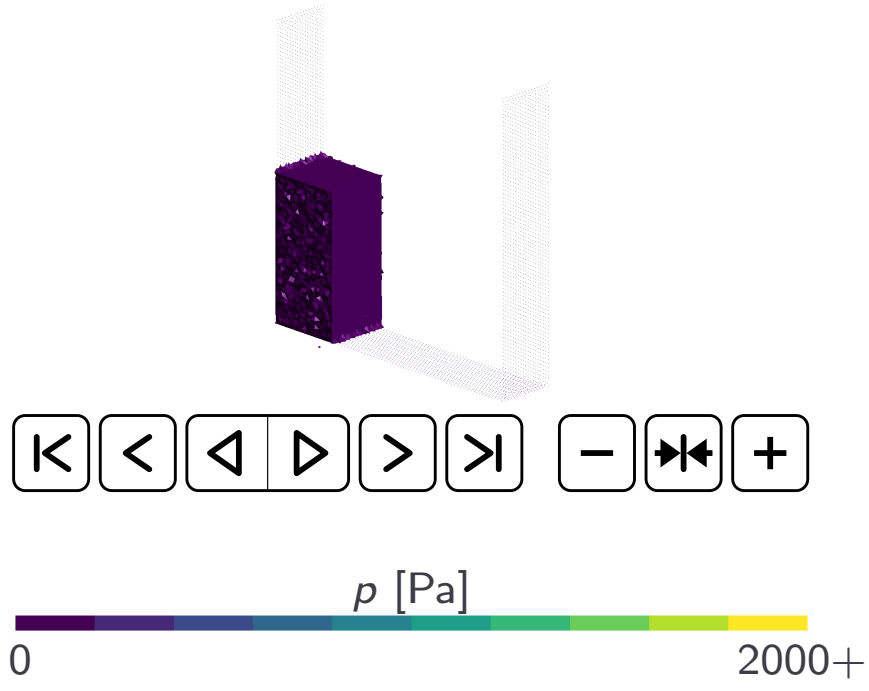

Development of a 3D compressible flow solver for PFEM fluid simulations

Software used: `C++`, `OpenMP`, `Eigen`, `GMSH`, `CGAL`, `Lua`

Master Thesis

Engineering physics master thesis: first prototype of **3D** Newtonian flow solver using PFEM (from scratch, no thermal effect).

Poiseuille flow in pipe

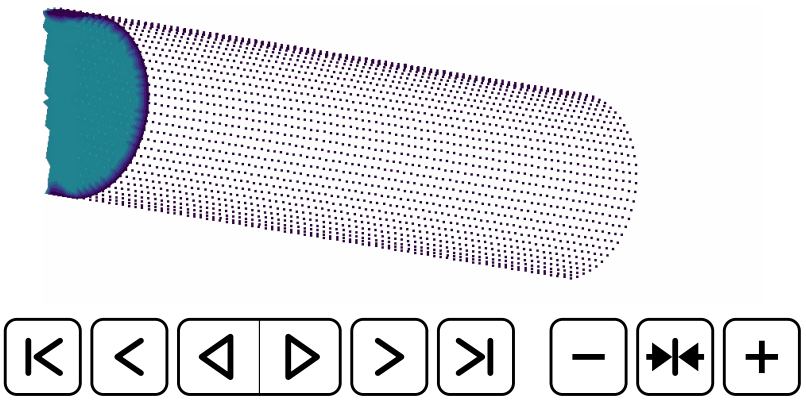

Dam break

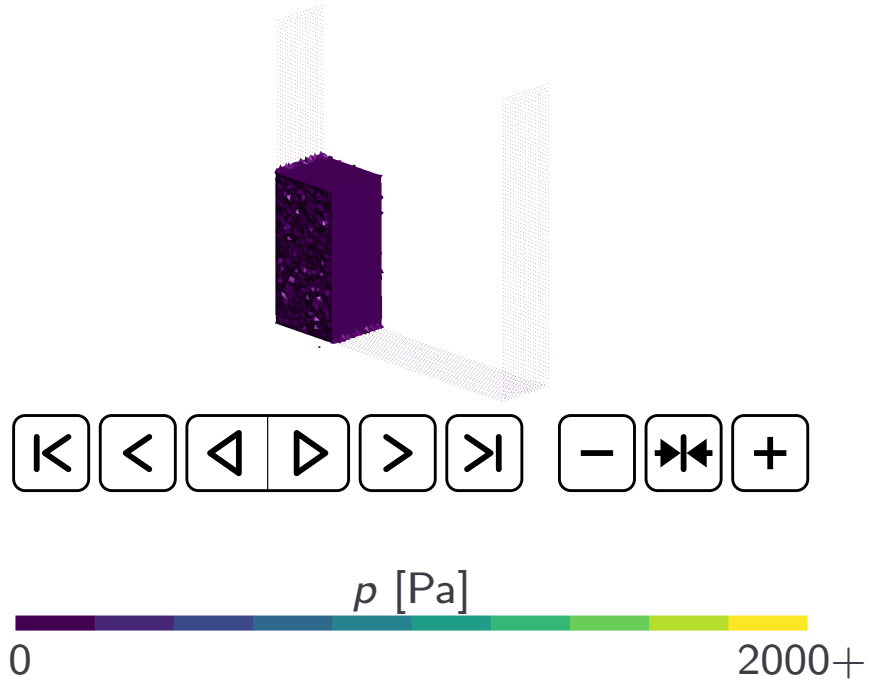

Development of a 3D compressible flow solver for PFEM fluid simulations

Software used: `C++`, `OpenMP`, `Eigen`, `GMSH`, `CGAL`, `Lua`

October-December work – Help-FRIA-A

Boussinesq problem simulation using PFEM (first thermal coupling):

- imposed ΔT between two plates in presence of gravity,
- $\Delta T > \Delta T_{crit} \rightarrow$ instabilities and apparition of "convection cells".

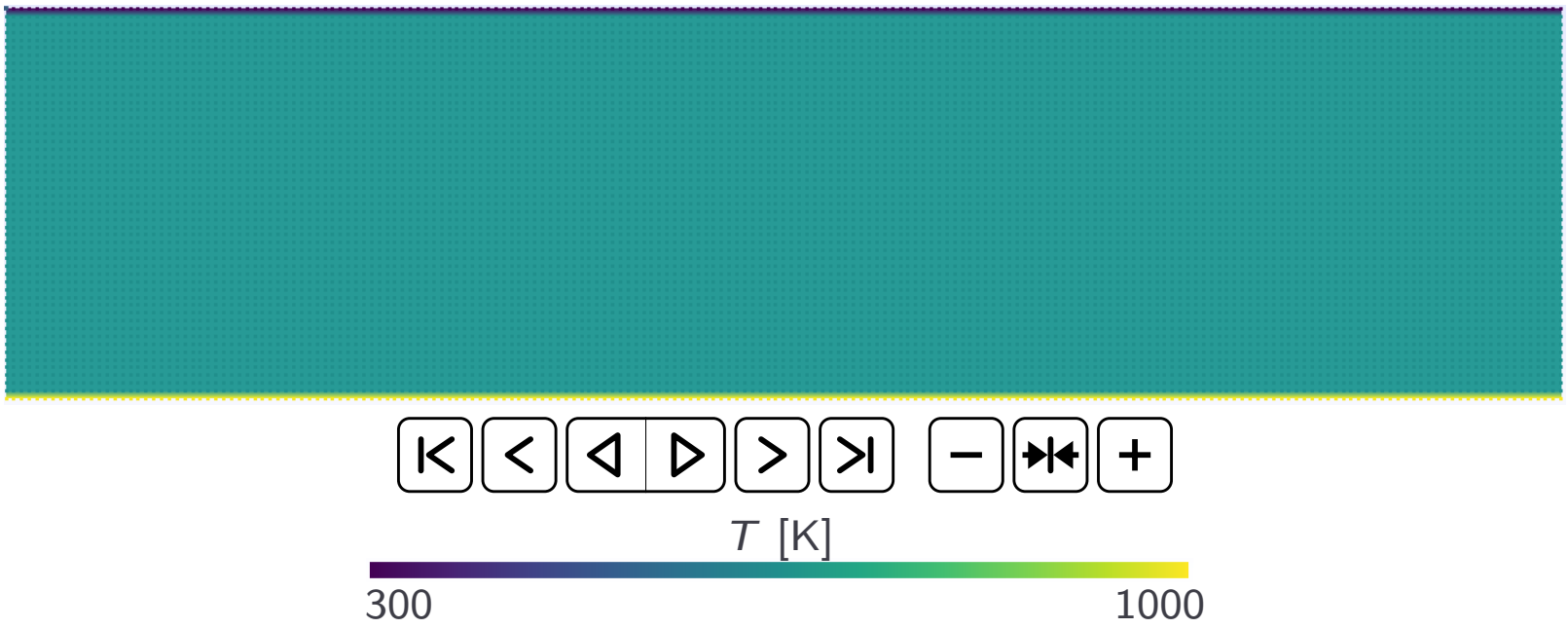

October-December work – Help-FRIA-A

Boussinesq problem simulation using PFEM (first thermal coupling):

- imposed ΔT between two plates in presence of gravity,
- $\Delta T > \Delta T_{crit} \rightarrow$ instabilities and apparition of "convection cells".

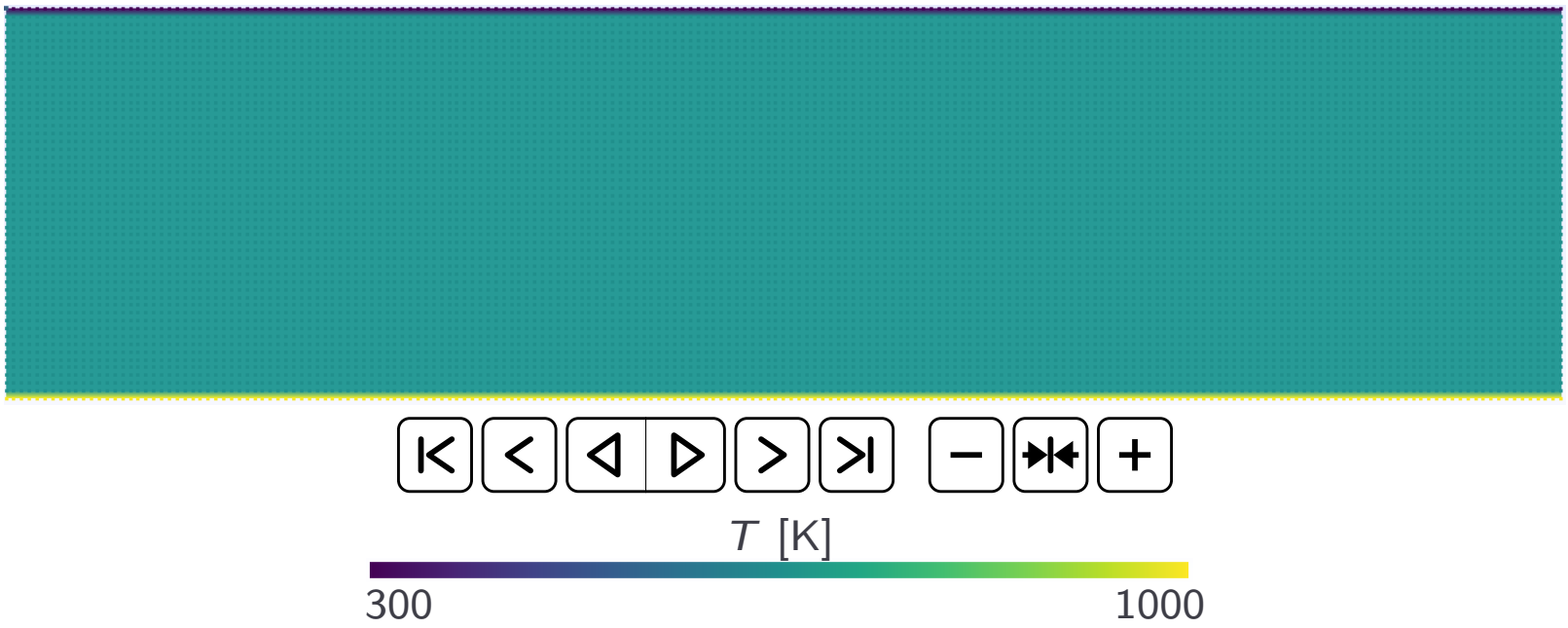

October-December work – Help-FRIA-A

Curvature computation in 3D → surface tension → cube of fluid to sphere without gravity (Laplace pressure).
$p_{theo} = 3.224\,\text{Pa}$. $p_{num} = 3.17\,\text{Pa}$.

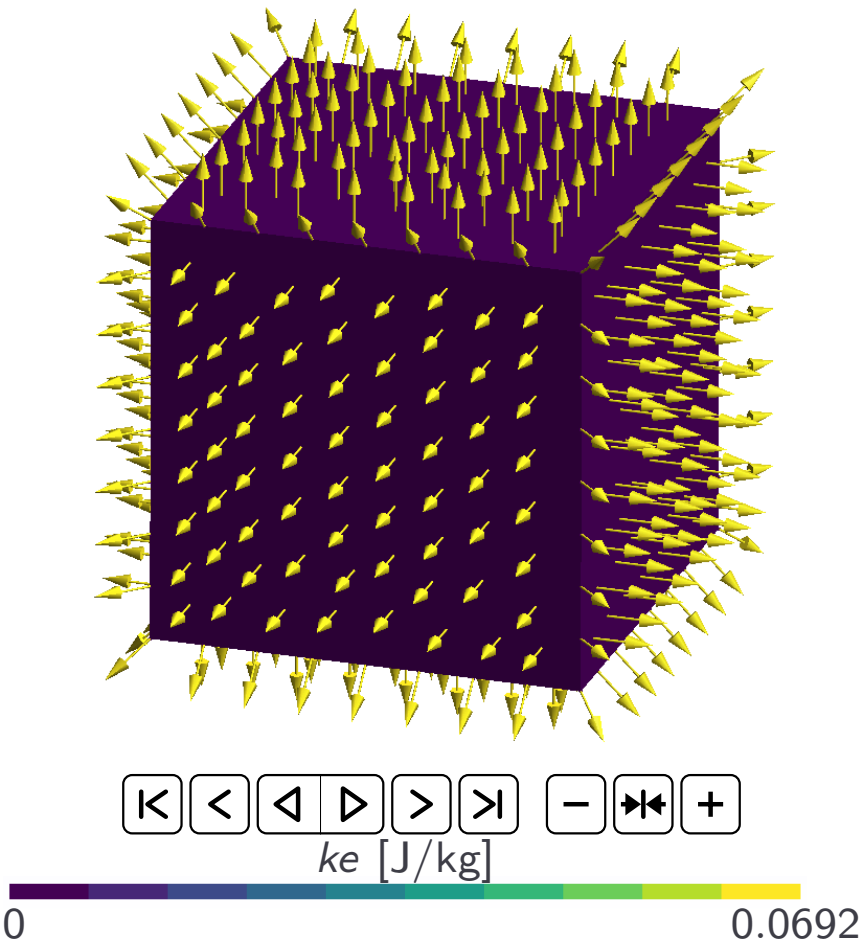

October-December work – Help-FRIA-A

Curvature computation in 3D → surface tension → cube of fluid to sphere without gravity (Laplace pressure).
$p_{theo} = 3.224\,\text{Pa}$. $p_{num} = 3.17\,\text{Pa}$.

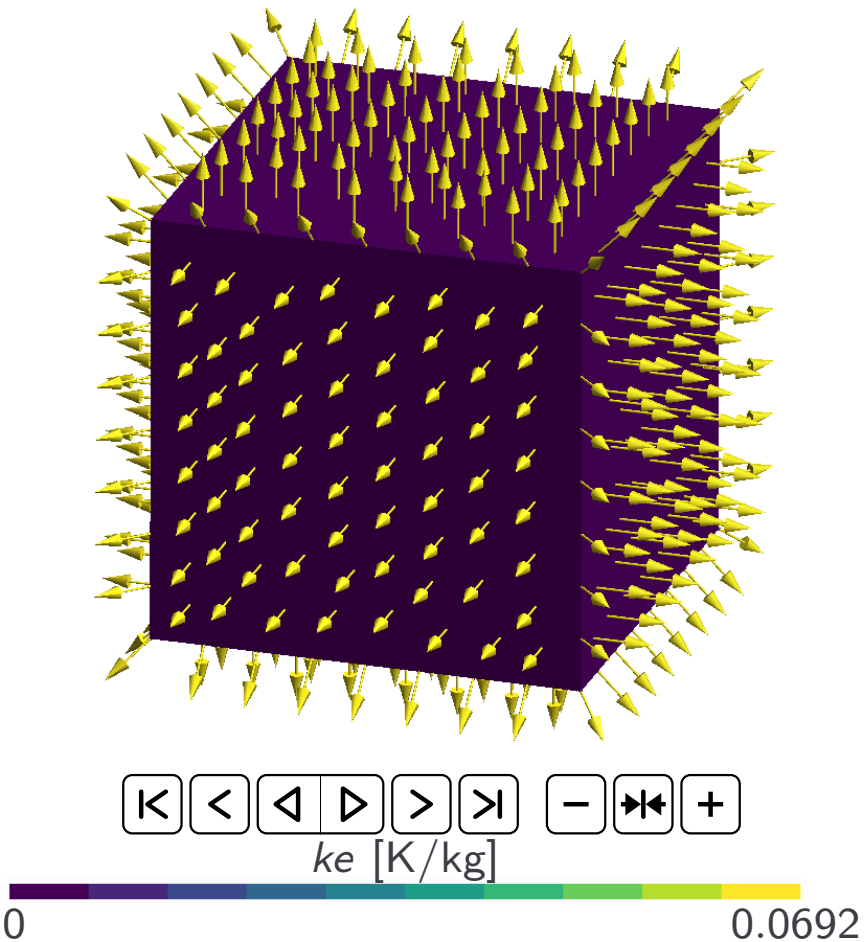

Conclusions

Conclusions

1. **3D** keyhole instabilities modelling needed by industrials to improve performance and productivity.

2. Current state of the art method quite complex and unable to model the whole phenomenon.

3. Original **3D** extension of the **PFEM** method proposed in order to solve those issues.

4. Candidate has the coding and physics skills available to implement this project.

Questions ?

Appendices

References

Li et al.

Balling behavior of stainless steel and nickel powder during selective laser melting process.
Journal of Materials Processing Technology, 59(9-12):1025–1035, Apr. 2012.

Gunenthiram et al.

Experimental analysis of spatter generation and melt-pool behavior during the powder bed laser beam melting process.
Journal of Materials Processing Technology, 251:376–386, Jan. 2018.

Caprio et al.

Observing molten pool surface oscillations during keyhole processing in laser powder bed fusion as a novel method to estimate the penetration depth.
Additive Manufacturing, 36:101470, May 2020.

C. Kusuma.

The Effect of Laser Power and Scan Speed on Melt Pool Characteristics of Pure Titanium and Ti-6Al-4V Alloy for Selective Laser Melting.
PhD thesis, Wright State University, 2016.

Q. Chen.

Thermomechanical numerical modelling of additive manufacturing by selective laser melting of powder bed: Application to ceramic materials.
PhD thesis, Université de recherche Paris Sciences et Lettres, 2018.

Gong et al.

Melt Pool Characterization for Selective Laser Melting of Ti-6Al-4V Pre-Alloyed Powder.
Proceedings, 2014.

Cook et al.

Simulation of Melt Pool Behaviour during Additive Manufacturing: Underlying Physics and Progress.
Additive Manufacturing, 31:10909, Jan 2020.

Detrimental effects

1) **Balling**: continuous tracks switch to tracks of spheres at **too high scan speed** $\rightarrow$ porosities.

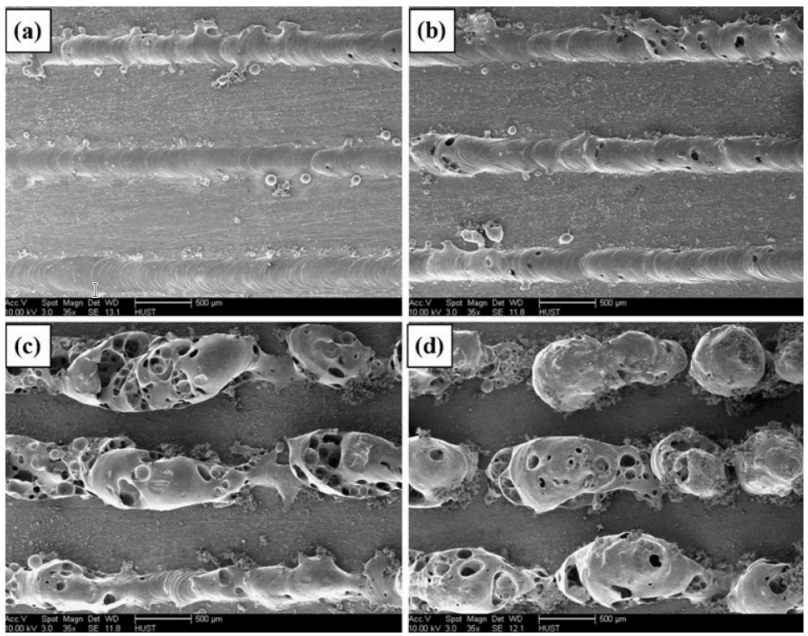

From Li et al. 2012.

2) **Spattering**: ejection of matter from the melt pool at **too high laser power** $\rightarrow$ contamination of the powder bed.

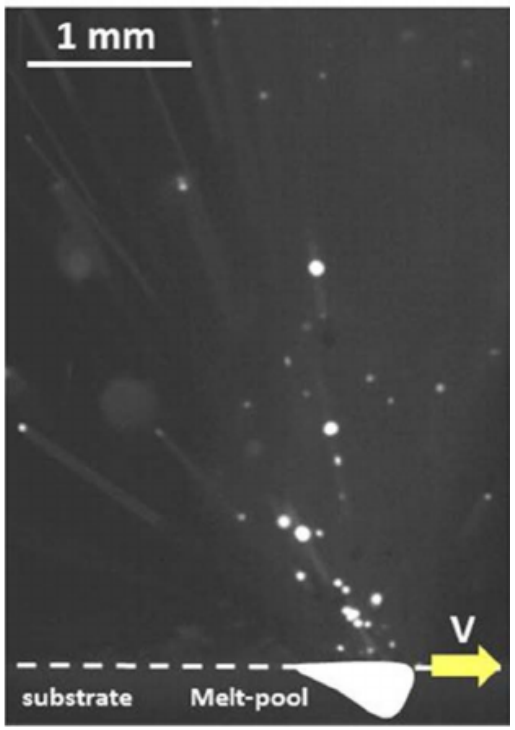

From Gunenthiram, et al. 2017.

Other previous work

Multiphysics integrated computational project (C. Geuzaine et R. Boman): DG-FEM solver for non-linear shallow water equations on unstructured meshes.

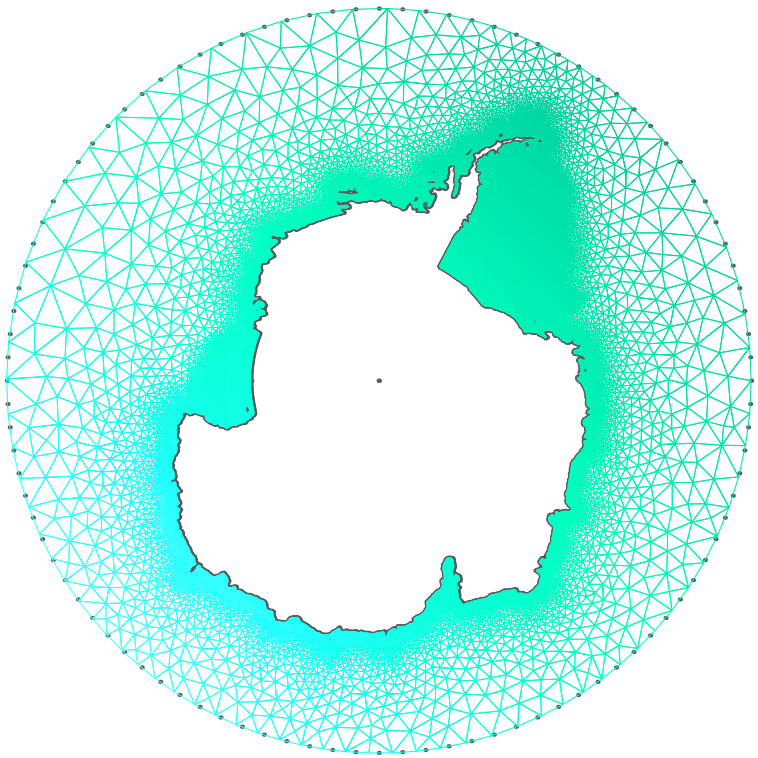

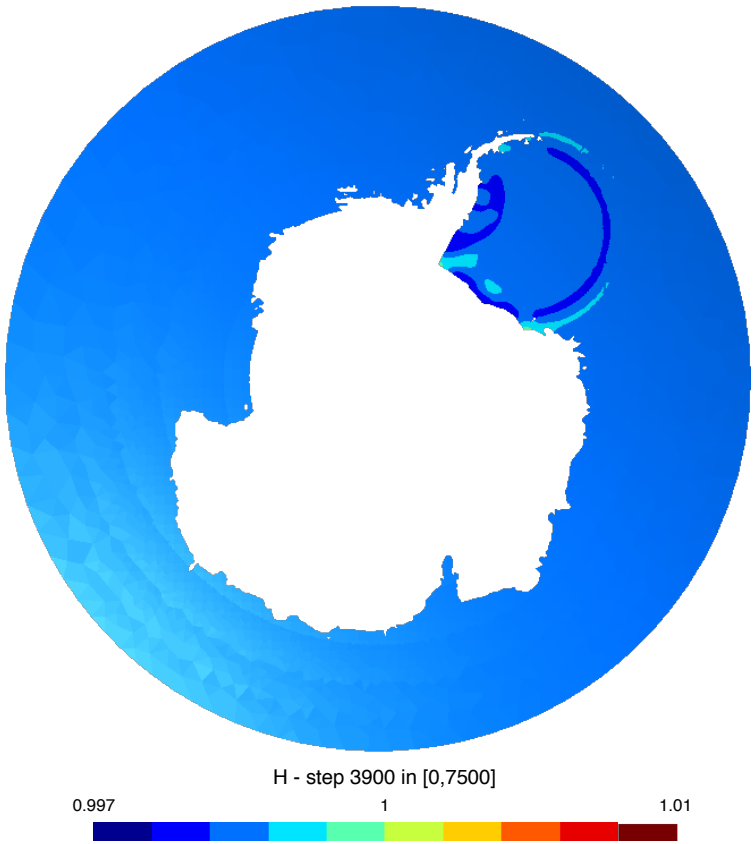

The Discontinuous Galerkin method - Application to shallow water equations

Software used: `C++`, `OpenMP`, `Eigen`, `GMSH`

Work environment (partim)

B.-J. Bobach, FRIA grant, working on shallow weld pool solidification using PFEM in 2D (axisymmetric figure).

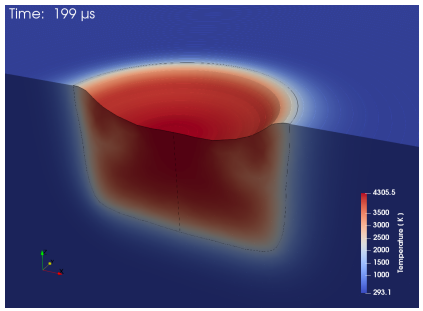

P.-L. Valkenborgh and E. Fernandez, AIFeWeld, working on friction melt bonding, using PFEM.

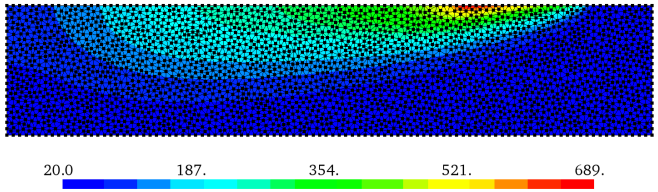

Cedric Laruelle, teaching assistant, working on macroscopic aspects of additive manufacturing.

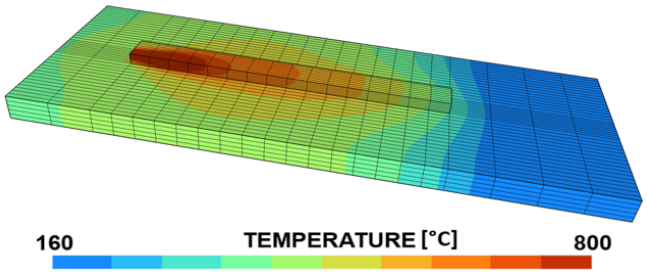

Romain Falla, PDR FNRS, working on adaptative remeshing in PFEM.

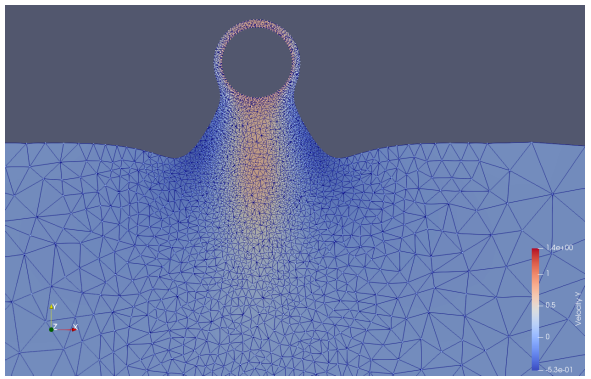

Comparison with B.-J. Bobach works

B.-J. Bobach

Shallow weld pool solidification:

- 2D,
- phases changes (melting, solidification but no vaporization),
- solid mechanic aspects,
- final residual stresses,
- geometrical distortions.

S. Février

Keyhole instabilities:

- 3D and HPC aspects.
- when is the keyhole wall unstable ?
- why is the keyhole wall unstable ?
- must also include vaporization and recoil pressure.

Characteristic scales

- flow velocity: $0.5\,\mathrm{m\,s^{-1}}$,
- powder thickness: $50\,\mu\mathrm{m}$,
- layer thickness: $30\,\mu\mathrm{m}$,
- melt pool depth: $200\,\mu\mathrm{m}$,
- liquid lifetime: $100\,\mu\mathrm{s}$,
- laser spot diameter: $50\,\mu\mathrm{m}$,
- laser spot speed: 50-400 $\mathrm{mm\,s^{-1}}$,
- laser power: 40-200 W
- $Re < 10$

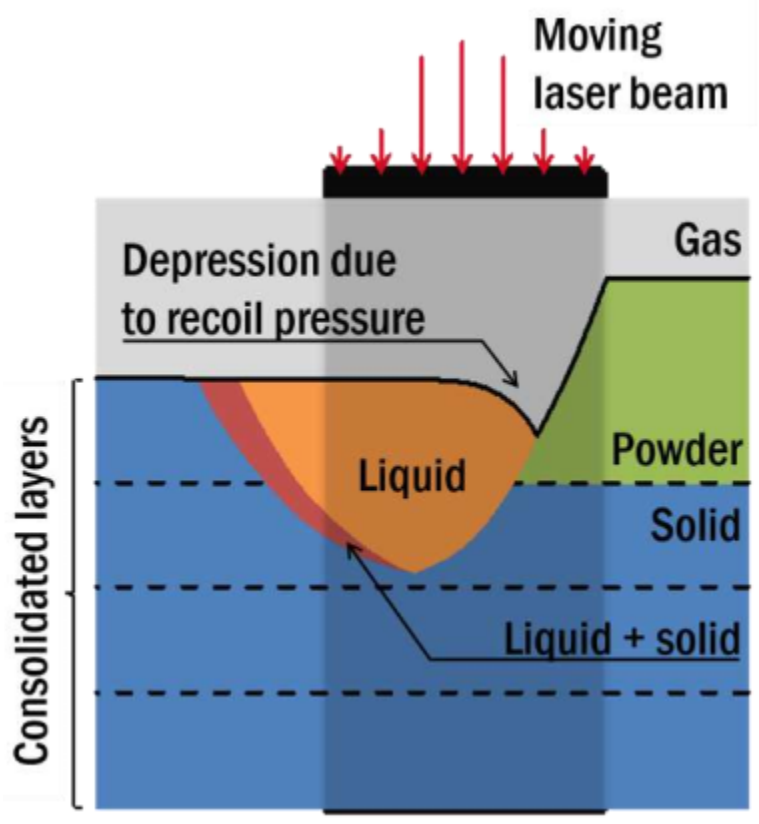

Melt pool dynamics. Adapted from Chen 2018.

Work plan

Work plan calendar

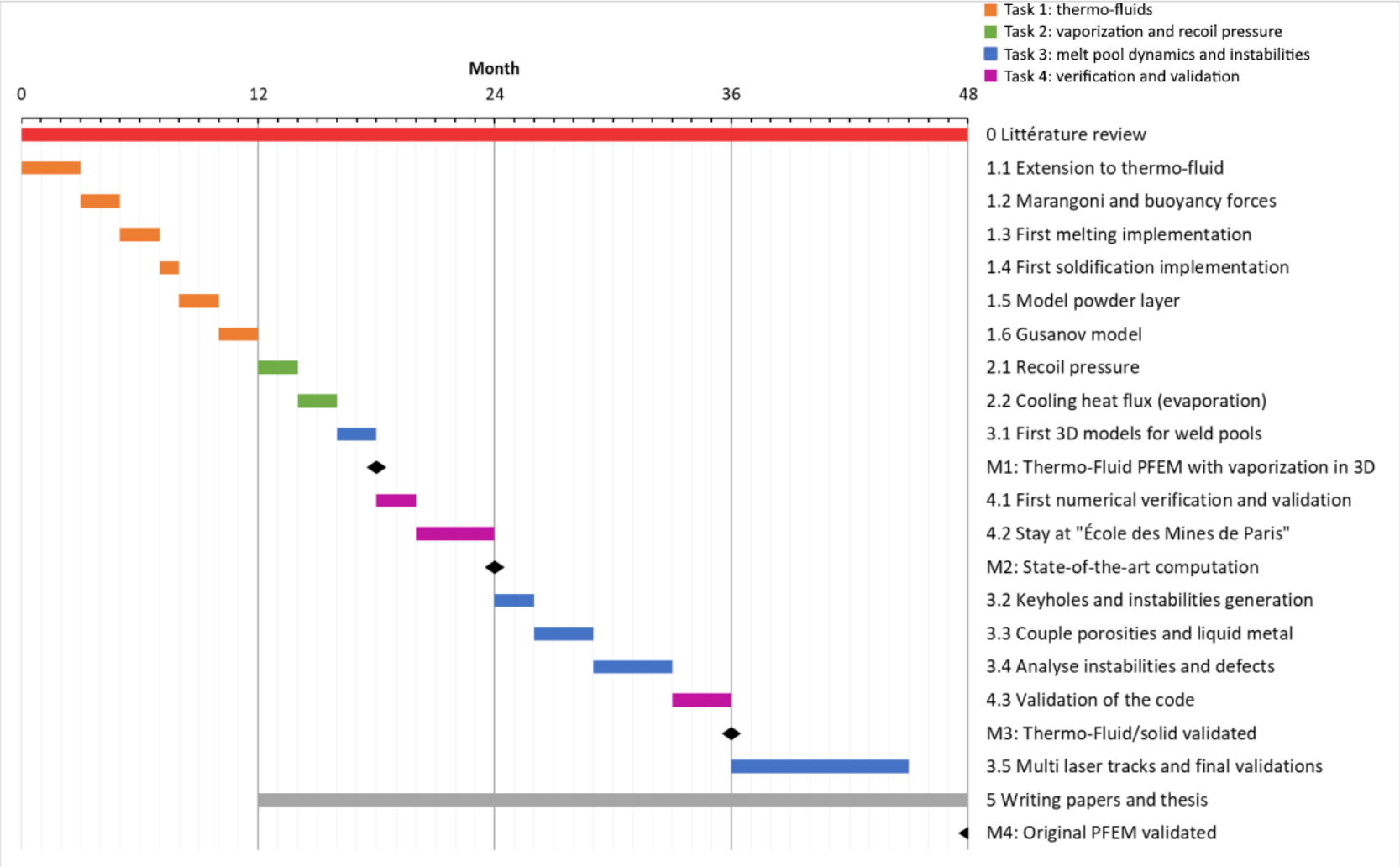

Basic physical ingredients

1.1 Extension of Navier–Stokes equations to thermo-fluid

Newtonian incompressible flow:

Continuity eq. :	$\vec{\nabla} \cdot \vec{v} = 0$	$\forall \vec{x} \in V$
Momentum eq. :	$\rho(T)\frac{d}{dt}\vec{v} = \vec{\nabla} \cdot \vec{\vec{\sigma}} + \rho(T)\vec{b}$	$\forall \vec{x} \in V$
Energy eq. :	$\rho(T)\frac{d}{dt}u = \vec{\vec{\sigma}} : \vec{\vec{D}} - \vec{\nabla} \cdot \vec{q} + \rho(T)r$	$\forall \vec{x} \in V$
Constitutive eq. :	$\vec{\vec{\sigma}} = -p\vec{\vec{I}} + 2\mu(T)\mathrm{dev}\vec{\vec{D}}$	$\forall \vec{x} \in V$
Fourrier's law :	$\vec{q} = -k(T)\vec{\nabla} T$	$\forall \vec{x} \in V$

Boundary conditions:

Imposed velocity:	$\vec{v} = \vec{v}_b$	$\forall \vec{x} \in S_{D,v}$
Imposed surface traction:	$\vec{\vec{\sigma}} \cdot \hat{n} = \gamma(T)\kappa\hat{n} - \vec{\nabla}\gamma\Big\|_S$	$\forall \vec{x} \in S_{N,v}$
Imposed temperature:	$T = T_b$	$\forall \vec{x} \in S_{D,T}$
Imposed heat flux:	$\vec{q} = \vec{q}_b$	$\forall \vec{x} \in S_{N,T}$

1.2 Marangoni and buoyancy forces

From free surface boundary condition:

$$\vec{t} = \vec{\vec{\sigma}} \cdot \hat{n} = \underbrace{\gamma(T)\kappa\hat{n}}_{\text{normal contribution}} - \underbrace{\vec{\nabla}\gamma\Big|_s}_{\text{tangential contribution}}$$

with γ the **surface tension** κ the free surface **curvature** and $\hat{n}$ the unit outward **normal**. **Marangoni forces** from gradient of surface tension along the free surface:

$$\gamma(T) = \gamma_0 + \left.\frac{d\gamma}{dT}\right|_{T_0}(T - T_0)$$

$$\Rightarrow \vec{\nabla}\gamma\Big|_s = \left.\frac{d\gamma}{dT}\right|_{T_0}\vec{\nabla}T\Big|_s = \left.\frac{d\gamma}{dT}\right|_{T_0}(\vec{\nabla}T - (\vec{\nabla}T \cdot \hat{n})\hat{n})$$

N.B.: $\vec{\nabla}\gamma\Big|_s = 0$ if $\vec{\nabla}T\Big|_s = 0$

Buoyancy volumic forces from temperature dependent density:

$$\rho = \rho_0(1 - \alpha(T - T_0))$$

1.3 First melting implementation (simplified approach)

Melting: **liquid fraction** $f_l \in [0,1]$ and **solid fraction** $f_s \in [0,1]$ such that $f_l + f_s = 1$, with:

$$f_l(T) = \begin{cases} 0 & T \leq T_s \\ \dfrac{T - T_s}{T_l - T_s} & T_s \leq T \leq T_l \\ 1 & T \geq T_l \end{cases}$$

with T_s the **solidus** temperature and T_l the **liquidus** temperature, and:

$$h = \int_0^T c_p(T^\star) dT^\star + f_l(T) L_m$$

with h the **specific enthalpy**, c_p the specific heat capacity at constant pressure and L_m the latent heat of melting.

1.4 First solidification implementation (simplified approach)

Darcy volumic forces: Artificial (numerical) freeze of the solid part.

Mushy zone: when $T_s \leq T \leq T_l$, porous medium with liquid and solid phase in equilibrium, drag force on the flow:

$$\vec{f}_{Darcy} = -\frac{C(1-f_l)^2}{f_l^3 + \varepsilon}\vec{v}$$

$\varepsilon \ll 1$ to avoid division by zero, C large enough to freeze fluid when $T \to T_s$. **Solid phase** when $T \leq T_s \Rightarrow f_l = 0 \Rightarrow \vec{f}_{Darcy} = -\frac{C}{\varepsilon}\vec{v}$.

Future: unified model fluid $\to$ mushy $\to$ solid: see Koeune, Ponthot [2014], International Journal of Plasticity.

1.5 Model powder layer as continuum

Mechanical properties averaged between fraction of powder and fraction of gas, but **thermal conductivity** works differently:

$$k = k_r + k_s + k_g$$

where k_r represents inter-particle interaction, k_s is particle-particle interaction and k_g is particle-gas interaction:

$$k_r = \frac{16}{3} L \sigma_b T^3$$

$$k_s = \frac{\Lambda a}{r} k_m$$

$$k_g = \frac{(1+f_m)(2+f_m)}{(1-f_m)(2-f_m)} k_{gas}$$

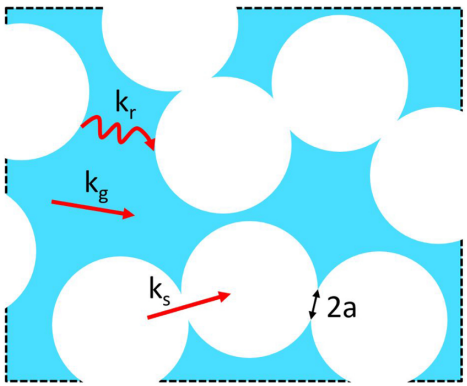

From Cook et al. 2019.

L: photon mean free path, σ_b Boltzmann constant, r: particle radius, a: connecting neck radius, k_m: metal bulk conductivity, Λ geometrical constant, f_m: solid volume fraction, k_{gas}: gas conductivity.

1.6 Gusarov model

Gusarov heat source:

$$P(t,r,z) = P(t) I_{rad}(r) I_{dep}(z)$$

$$I_{rad}(r) = \frac{3}{\pi R^2}\left(1-\frac{r}{R}\right)^2\left(1+\frac{r}{R}\right)^2$$

$$I_{dep}(z) = -\beta(r)\frac{dq}{d\xi(z)}$$

$$\xi(z) = \beta z$$

$$\beta = \frac{3(1-\varepsilon_b)}{2\varepsilon_b D}$$

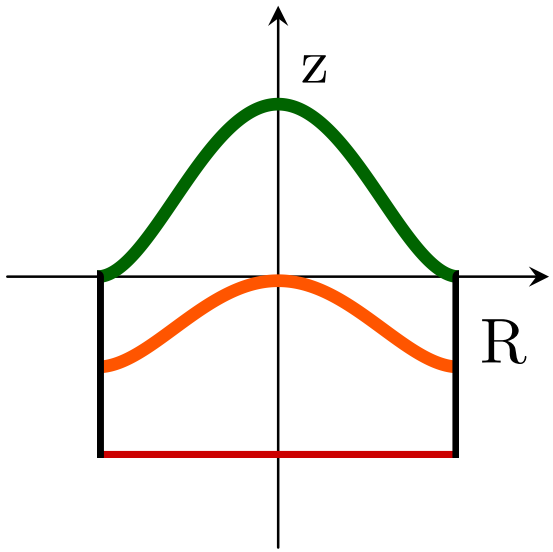

R: laser radius, β: optical extinction coefficient, ε_b: powder bed porosity, D: particle diameter, $P(t)$: maximum laser power.

See Gusarov et al, *Model of Radiation and Heat Transfer in Laser-Powder Interaction Zone at Selective Laser Melting*, Journal of Heat Transfer, 2009

2. Recoil pressure and cooling heat flux

Vapour saturation pressure resulting from vaporization of metallic material :

$$P_s(T) \simeq P_{atm} \exp\left(\frac{L_v m_A (T - T_b)}{k_B T T_b}\right)$$

L_v: latent heat of vaporization, T_b: boiling temperature, k_B: the Boltzmann constant, m_A the atomic mass, P_{atm}: surrounding pressure for inert gas.

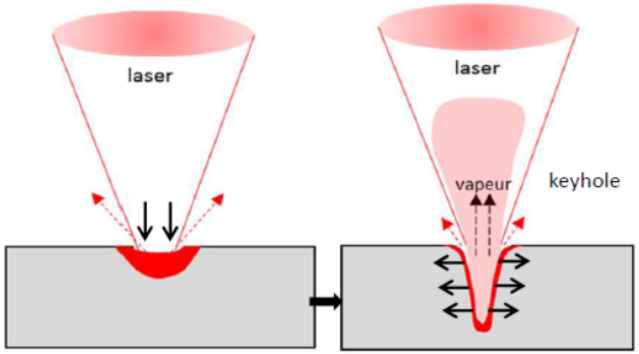

From *Physics of Additive Manufacturing processes with Lasers*, P. Peyre, St-Petersburg University, lecture notes

Recoil pressure:

$$P_{rec}(T) \simeq 0.56 P_s(T)$$

Energy removal from net flux of vapour going out of the material (Clausius-Clapeyron empirical equation):

$$r_{evap} = 0.82 L_v \sqrt{\frac{m_A}{2\pi k_B T}} P_s$$

See Cook et al. 2019.

3.1 First 3D model for weld pool dynamics

Milestone $t_0 + 18$ months:

- thermo-fluid code,
- Marangoni, buoyancy and Darcy forces,
- melting/solidification,
- continuum powder layer,
- Gusarov model of laser,

} after one year

- recoil pressure,
- heat from evaporation taken into account

} six months more

$\rightarrow$ first **3D** models for weld pool dynamics.

3.2 Keyholes and instabilities generation

Integrate PFEM fluid with PFEM solid (B.-J. Bobach) for whole solid/liquid + vaporization spectrum $\rightarrow$ high laser power and keyholes.

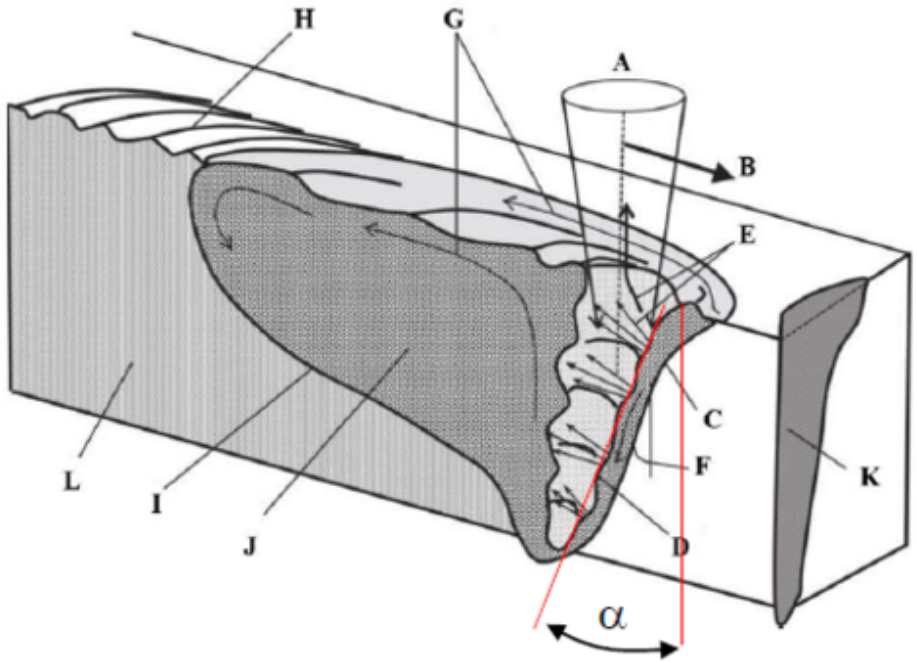

From *Physics of Additive Manufacturing processes with Lasers*, P. Peyre, St-Petersburg University, lecture notes

3.3 Couple porosities and liquid metal

Porosities modelled generally as incompressible volume $\rightarrow$ small compressible gas model for porosities and fluid-fluid coupling through CuPyDo.

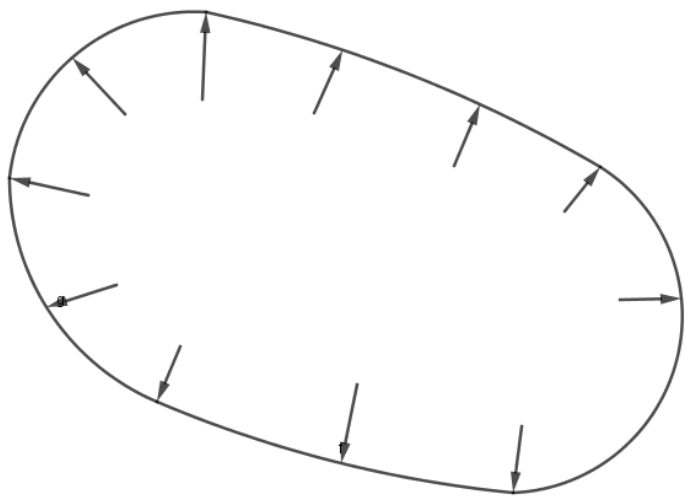

The gas inside the pore exert a pressure on the pore's wall.

Space and time discretization using PFEM

Weak form of the Navier–Stokes equations

Newtonian flow:

Continuity eq. :	$\frac{d}{dt}\rho(T) + \rho(T)\vec{\nabla}\cdot\vec{v} = 0$	$\forall\vec{x} \in V$
Momentum eq. :	$\rho(T)\frac{d}{dt}\vec{v} = \vec{\nabla}\cdot\vec{\vec{\sigma}} + \rho(T)\vec{b}$	$\forall\vec{x} \in V$
Energy eq. :	$\rho(T)\frac{d}{dt}u = \vec{\vec{\sigma}} : \vec{\vec{D}} - \vec{\nabla}\cdot\vec{q} + \rho(T)r$	$\forall\vec{x} \in V$
Constitutive eq. :	$\vec{\vec{\sigma}} = -p\vec{\vec{I}} + 2\mu(T)\mathrm{dev}\vec{\vec{D}}$	$\forall\vec{x} \in V$
Fourrier's law :	$\vec{q} = -k(T)\vec{\nabla}T$	$\forall\vec{x} \in V$

Boundary conditions:

Imposed velocity:	$\vec{v} = \vec{v}_b$	$\forall\vec{x} \in S_{D,v}$
Imposed surface traction:	$\vec{\vec{\sigma}}\cdot\hat{n} = \gamma(T)\kappa\hat{n} - \vec{\nabla}\gamma\Big\vert_S$	$\forall\vec{x} \in S_{N,v}$
Imposed temperature:	$T = T_b$	$\forall\vec{x} \in S_{D,T}$
Imposed heat flux:	$\vec{q} = \vec{q}_b$	$\forall\vec{x} \in S_{N,T}$

Weak form of the Navier–Stokes equations – cont'd

Let's first concentrate on a temperature independent incompressible fluid. We multiply each equation by a test function φ, $\vec{\phi}$ and we integrate over the whole volume (stress derivatives eliminated using integration by parts):

$$\begin{cases} \displaystyle\int_{V(t)} \varphi\, \vec{\nabla}\cdot\vec{v}\, dV = 0, & \forall \vec{x} \in V(t) \\ \displaystyle\int_{V(t)} \vec{\phi}\cdot\rho\frac{d\vec{v}}{dt}\, dV = -\int_{V(t)} \vec{\nabla}\vec{\phi}\colon\vec{\vec{\sigma}}\, dV + \int_{V(t)} \vec{\phi}\cdot\rho\vec{b}\, dV + \int_{S_N(t)} \vec{\phi}\cdot\vec{t}_b\, dS_N, & \forall \vec{x} \in V(t) \\ \vec{v}(\vec{X}, t=0) = \vec{v}_0 \text{ and } \rho(\vec{X}, t=0) = \rho_0, & \forall \vec{X} \in V(t=0) \\ \vec{v}(\vec{x}, t) = \vec{v}_b, & \forall \vec{x} \in S_D(t) \end{cases}.$$

where $\vec{t}_b = \gamma\kappa\hat{n} - \vec{\nabla}\gamma\Big|_S$. (Marangoni forces)

Galerkin formulation - cont'd

We discretize the weak form and the test functions using the same space discretization:

$$\begin{aligned} &\text{Velocity:} && \vec{v} = \tilde{\mathbf{N}}\mathbf{v} \\ &\text{Pressure:} && p = \mathbf{N}\mathbf{p} \end{aligned}$$

using **tetrahedra**, with (nodal unknowns):

$$\mathbf{v} = \begin{pmatrix} u_1 & u_2 & u_3 & u_4 & v_1 & v_2 & v_3 & v_4 & w_1 & w_2 & w_3 & w_4 \end{pmatrix}^{\mathsf{T}}$$

$$\mathbf{p} = \begin{pmatrix} p_1 & p_2 & p_3 & p_4 \end{pmatrix}^{\mathsf{T}}$$

Galerkin formulation

We introduce the following matrices of shape functions (3D):

$$\mathbf{N} = \begin{bmatrix} N_1 & N_2 & N_3 & N_4 \end{bmatrix} \qquad \tilde{\mathbf{N}} = \begin{bmatrix} \mathbf{N} & \mathbf{0} & \mathbf{0} \\ \mathbf{0} & \mathbf{N} & \mathbf{0} \\ \mathbf{0} & \mathbf{0} & \mathbf{N} \end{bmatrix}$$

$$\nabla \mathbf{N} = \begin{bmatrix} \frac{\partial N_1}{\partial x} & \frac{\partial N_2}{\partial x} & \frac{\partial N_3}{\partial x} & \frac{\partial N_4}{\partial x} \\ \frac{\partial N_1}{\partial y} & \frac{\partial N_2}{\partial y} & \frac{\partial N_3}{\partial y} & \frac{\partial N_4}{\partial y} \\ \frac{\partial N_1}{\partial z} & \frac{\partial N_2}{\partial z} & \frac{\partial N_3}{\partial z} & \frac{\partial N_4}{\partial z} \end{bmatrix}$$

Galerkin formulation - cont'd

$$\mathbf{B} = \begin{bmatrix} \frac{\partial N_1}{\partial x} & \frac{\partial N_2}{\partial x} & \frac{\partial N_3}{\partial x} & \frac{\partial N_4}{\partial x} & 0 & 0 & 0 & 0 & 0 & 0 & 0 & 0 \\ 0 & 0 & 0 & 0 & \frac{\partial N_1}{\partial y} & \frac{\partial N_2}{\partial y} & \frac{\partial N_3}{\partial y} & \frac{\partial N_4}{\partial y} & 0 & 0 & 0 & 0 \\ 0 & 0 & 0 & 0 & 0 & 0 & 0 & 0 & \frac{\partial N_1}{\partial z} & \frac{\partial N_2}{\partial z} & \frac{\partial N_3}{\partial z} & \frac{\partial N_4}{\partial z} \\ \frac{\partial N_1}{\partial y} & \frac{\partial N_2}{\partial y} & \frac{\partial N_3}{\partial y} & \frac{\partial N_4}{\partial y} & \frac{\partial N_1}{\partial x} & \frac{\partial N_2}{\partial x} & \frac{\partial N_3}{\partial x} & \frac{\partial N_4}{\partial x} & 0 & 0 & 0 & 0 \\ \frac{\partial N_1}{\partial z} & \frac{\partial N_2}{\partial z} & \frac{\partial N_3}{\partial z} & \frac{\partial N_4}{\partial z} & 0 & 0 & 0 & 0 & \frac{\partial N_1}{\partial x} & \frac{\partial N_2}{\partial x} & \frac{\partial N_3}{\partial x} & \frac{\partial N_4}{\partial x} \\ 0 & 0 & 0 & 0 & \frac{\partial N_1}{\partial z} & \frac{\partial N_2}{\partial z} & \frac{\partial N_3}{\partial z} & \frac{\partial N_4}{\partial z} & \frac{\partial N_1}{\partial y} & \frac{\partial N_2}{\partial y} & \frac{\partial N_3}{\partial y} & \frac{\partial N_4}{\partial y} \end{bmatrix}$$

NB: we also have $\nabla \mathbf{N}\,\mathbf{p} = \begin{pmatrix} \frac{\partial p}{\partial x} & \frac{\partial p}{\partial y} & \frac{\partial p}{\partial z} \end{pmatrix}^{\mathsf{T}}$ and

$\mathbf{Bv} = \begin{pmatrix} \frac{\partial u}{\partial x} & \frac{\partial v}{\partial y} & \frac{\partial w}{\partial z} & \frac{\partial u}{\partial y} + \frac{\partial v}{\partial x} & \frac{\partial u}{\partial z} + \frac{\partial w}{\partial x} & \frac{\partial v}{\partial z} + \frac{\partial w}{\partial y} \end{pmatrix}^{\mathsf{T}}$

Discrete incompressible Newtonian flow equations

Discrete version of incompressible Newtonian flow equations:

Momentum equation:
$$\mathbf{M}_{\rho_0}\frac{d}{dt}\mathbf{v} = -\underbrace{\mathbf{K}_\mu \mathbf{v}}_{\text{viscous forces}} + \underbrace{\mathbf{D}^\mathsf{T}\mathbf{p}}_{\text{pressure forces}} + \mathbf{f}_{\text{ext}}$$

Incompressibility constraint: $\mathbf{D}\mathbf{v} = \mathbf{0}$

with:

$$\mathbf{M}_{\rho_0} = \int_{\Omega(t)} \rho_0 \tilde{\mathbf{N}}^\mathsf{T}\tilde{\mathbf{N}}\, d\Omega \qquad \mathbf{K}_\mu = \int_{\Omega(t)} \mu \mathbf{B}^\mathsf{T}\mathbf{d}_{\text{dev}}\mathbf{B}\, d\Omega$$

$$\mathbf{D} = \int_{\Omega(t)} \mathbf{N}^\mathsf{T}\mathbf{m}^\mathsf{T}\mathbf{B}\, d\Omega \qquad \mathbf{f}_{\text{ext}} = \int_{\Omega(t)} \rho_0 \tilde{\mathbf{N}}^\mathsf{T}\vec{b}\, d\Omega + \int_{\Gamma(t)} \tilde{\mathbf{N}}^\mathsf{T}\vec{t}_b\, d\Gamma$$

$$\mathbf{d}_{\text{dev}} = \text{diag}(2,2,2,1,1,1) \qquad \mathbf{m}^\mathsf{T} = (1,1,1,0,0,0)$$

ρ_0: the density, μ: the viscosity, $\vec{b}$: body forces, $\vec{t}_b$: surface traction.

Discrete incompressible Newtonian flow equations – cont'd

Let's try a Euler backward scheme:

$$\begin{bmatrix} \frac{1}{\Delta t}\mathbf{M}_{\rho_0}^{n+1} + \mathbf{K}_{\mu}^{n+1} & \mathbf{D}^{\mathsf{T}\,n+1} \\ \mathbf{D}^{n+1} & \mathbf{0} \end{bmatrix} \begin{pmatrix} \mathbf{v}^{n+1} \\ \mathbf{p}^{n+1} \end{pmatrix} = \begin{bmatrix} \mathbf{f}_{\text{ext}}^{n+1} + \frac{1}{\Delta t}\mathbf{M}_{\rho_0}^{n+1}\mathbf{v}^{n} \\ \mathbf{0} \end{bmatrix}$$

Issues:

- saddle-point nature of the problem, pressure as Lagrange multiplier of the incompressibility constraint,
- linear velocity and pressure $\rightarrow$ violation of the LBB inf-sup condition $\rightarrow$ non-unique solution and oscillations.

Solution: PSPG stabilization

In the Pressure Stabilizing Petrov Galerkin (PSPG) procedure, the pair of test functions $(\varphi, \vec{\phi})$ is replaced by $(\varphi, \vec{\phi} + \tau\vec{\nabla}\varphi)$.

This leads to the following variational form for the continuity equation:

$$-\int_{V(t)} \varphi\vec{\nabla}\cdot\vec{v}\,dV + \int_{V(t)} \frac{\tau}{\rho}\vec{\nabla}\varphi\left(\rho\frac{d}{dt}\vec{v} - \vec{\nabla}\cdot\vec{\vec{\sigma}} - \rho\vec{b}\right)\,dV$$

from Hughes et al., *A new finite element formulation for computational fluid dynamics. V. Circumventing the Babuska-Brezzi condition: a stable Petrov-Galerkin formulation of the Stokes problem accommodating equal-order interpolations.*, Comput. Methods Appl.Mech. Engrg., 1986

Solution: PSPG stabilization

This acts like adding a term proportional to the momentum equation into the continuity equation:

- constant of proportionality τ,
- will tend to zero as we approach the exact solution.

$$\begin{cases} \mathbf{M}_{\rho_0} \dfrac{d}{dt}\mathbf{v} = -\mathbf{K}_\mu \mathbf{v} + \mathbf{D}^\mathsf{T}\mathbf{p} + \mathbf{f}_{\text{ext}} \\ \\ \mathbf{C}_\tau \dfrac{d}{dt}\mathbf{v} - \mathbf{D}\mathbf{v} + \mathbf{L}_{\tau/\rho_0}\mathbf{p} = \mathbf{h}_\tau \end{cases}$$

with:

$$\mathbf{C}_\tau = \int_{\Omega(t)} \tau \nabla \mathbf{N}^\mathsf{T} \tilde{\mathbf{N}}\, d\Omega \qquad \mathbf{L}_{\tau/\rho_0} = \int_{\Omega(t)} \frac{\tau}{\rho_0} \nabla \mathbf{N}^\mathsf{T} \nabla \mathbf{N}\, d\Omega$$

$$\mathbf{h}_\tau = \int_{\Omega(t)} \tau \nabla \mathbf{N}^\mathsf{T} \vec{b}\, d\Omega \qquad \tau = \sqrt{\frac{1}{(\frac{2}{\Delta t})^2 + (\frac{2\|U\|}{h})^2 + (\frac{4\mu}{h^2\rho})^2}}$$

τ: stabilization parameter, h: element characteristic size, $\|U\|$; element characteristic velocity magnitude.

Implicit backward Euler time integration

From discrete system of equations

$$\begin{cases} \mathbf{M}_\rho \dfrac{d}{dt}\mathbf{v} = -\mathbf{K}_\mu \mathbf{v} + \mathbf{D}^\mathsf{T}\mathbf{p} + \mathbf{f}_{\text{ext}} \\ \\ \mathbf{C}_\tau \dfrac{d}{dt}\mathbf{v} - \mathbf{D}_\tau \mathbf{v} + \mathbf{L}_{\tau/\rho}\mathbf{p} = \mathbf{h}_\tau \end{cases}$$

implicit Euler backward scheme:

$$\begin{bmatrix} \dfrac{1}{\Delta t}\mathbf{M}_\rho^{n+1} + \mathbf{K}_\mu^{n+1} & -\mathbf{D}^{\mathsf{T}\,n+1} \\ \\ \mathbf{C}_\tau^{n+1} - \mathbf{D}^{n+1} & \mathbf{L}_{\tau/\rho}^{n+1} \end{bmatrix} \begin{pmatrix} \mathbf{v}^{n+1} \\ \\ \mathbf{p}^{n+1} \end{pmatrix} = \begin{bmatrix} \mathbf{f}_{\text{ext}}^{n+1} + \dfrac{1}{\Delta t}\mathbf{M}_\rho^n \mathbf{v}^n \\ \\ \mathbf{h}_\tau^{n+1} \end{bmatrix}$$

Those non-linear equations have to be solved using a non-linear solver (e.g. Picard, Newton-Raphson, etc).

Explicit time integration

Discrete version of **weakly-compressible** Newtonian flow equations:

Momentum equation:
$$\mathbf{M}_\rho \frac{d}{dt}\mathbf{v} = -\mathbf{K}_\mu \mathbf{v} + \mathbf{D}^\mathsf{T}\mathbf{p} + \mathbf{f}_{\text{ext}}$$

Continuity equation:
$$\mathbf{M}\frac{d}{dt}\boldsymbol{\rho} + \mathbf{D}_\rho \mathbf{v} = 0 \quad \text{or} \quad \mathbf{M}\boldsymbol{\rho} = \mathbf{M}_0\boldsymbol{\rho}_0$$

Tait-Murnaghan equaton:
$$p = \frac{K_0}{K_0'}\left(\left(\frac{\rho}{\rho_0}\right)^{K_0'} - 1\right)$$

with:

$$\mathbf{M} = \int_{\Omega(t)} \mathbf{N}^\mathsf{T}\mathbf{N}\, d\Omega \qquad \mathbf{D}_\rho = \int_{\Omega(t)} \rho\mathbf{N}^\mathsf{T}\mathbf{m}^\mathsf{T}\mathbf{B}\, d\Omega$$

$$\mathbf{M}_\rho = \int_{\Omega(t)} \rho\tilde{\mathbf{N}}^\mathsf{T}\tilde{\mathbf{N}}\, d\Omega \qquad \mathbf{K}_\mu = \int_{\Omega(t)} \mu\mathbf{B}^\mathsf{T}\mathbf{d}_{\text{dev}}\mathbf{B}\, d\Omega$$

$$\mathbf{D} = \int_{\Omega(t)} \mathbf{N}^\mathsf{T}\mathbf{m}^\mathsf{T}\mathbf{B}\, d\Omega \qquad \mathbf{f}_{\text{ext}} = \int_{\Omega(t)} \rho\tilde{\mathbf{N}}^\mathsf{T}\vec{b}\, d\Omega + \int_{\Gamma(t)} \tilde{\mathbf{N}}^\mathsf{T}\vec{t}_b\, d\Gamma$$

$$\mathbf{m}^\mathsf{T} = (1,1,1,0,0,0) \qquad \mathbf{d}_{\text{dev}} = \text{block}\left(\begin{bmatrix} 4/3 & -2/3 & -2/3 \\ -2/3 & 4/3 & -2/3 \\ -2/3 & -2/3 & 4/3 \end{bmatrix}, \mathbf{I}\right)$$

Explicit time integration - Central Difference Scheme

We define:

- $\mathbf{f}^{n+1}_{momentum} = \mathbf{D}^{\mathsf{T}\,n+1}\mathbf{p}^{n} - \mathbf{K}^{n+1}_{\mu}\mathbf{v}^{n+1/2} + \mathbf{f}^{n+1}_{\text{ext}}$,
- $\mathbf{f}^{n+1}_{continuity} = \mathbf{M}^{n+1}_{\rho}\boldsymbol{\rho}^{n} - \Delta t^{n}\mathbf{D}^{n+1}_{\rho}\mathbf{v}^{n+1/2}$,
- K_e: the bulk modulus of element e.

Previous time step data: $(\mathbf{x}_n, \mathbf{v}_n, \mathbf{p}_n, \boldsymbol{\rho}_n, \mathbf{a}_n, \Delta t_n)$

Half-step velocity: $\mathbf{v}_{n+1/2} = \mathbf{v}_n + \frac{1}{2}\Delta t_n \mathbf{a}_n$

Position update: $\mathbf{x}_{n+1} = \mathbf{x}_n + \Delta t_n \mathbf{v}_{n+1/2}$

Density update: $\boldsymbol{\rho}_{n+1} = (\mathbf{M}^{n+1})^{-1}\mathbf{f}^{n+1}_{continuity}$

Pressure update: $\left[\mathbf{p}^{n+1}\right]_i = \frac{K_0}{K_0'}\left[\left(\frac{\left[\boldsymbol{\rho}^{n+1}\right]_i}{\rho_0}\right)^{K_0'} - 1\right] \quad \forall i$

Acceleration update: $\mathbf{a}_{n+1} = (\mathbf{M}^{n+1}_{\rho})^{-1}\mathbf{f}^{n+1}_{momentum}$

Velocity update: $\mathbf{v}_{n+1} = \mathbf{v}_{n+1/2} + \frac{1}{2}\Delta t_n \mathbf{a}_{n+1}$

Time step update: $\Delta t_{n+1} = C \min_e \left(\frac{h_e}{\max(\|U_e\|, \sqrt{K_e/\rho_e})}\right)$

Thermo-mechanical coupling – Energy equation

Hypothesis:

- $\vec{\vec{\sigma}} : \vec{\vec{D}} \approx 0$ (self-heating neglected),
- $u = \int_0^T c_V(T^\star)\, dT^\star$ (u = internal energy),
- $r = 0$ (no heat sources).

Energy conservation:

$$\rho c_v \frac{d}{dt} T = \vec{\nabla} \cdot (k \vec{\nabla} T) \qquad \forall \vec{x} \in V(t)$$

Boundary conditions:

$$T = T_b \qquad \forall \vec{x} \in S_{D,T}$$
$$\vec{q} = \vec{q}_b \qquad \forall \vec{x} \in S_{N,T}$$

Thermo-mechanical coupling – Weak form of energy equation

Weak form:

$$\int_{V(t)} \varphi \rho c_V \frac{d}{dt} T \, dV = -\int_{V(t)} \vec{\nabla}\varphi \cdot (k\vec{\nabla} T) \, dV + \int_{S_N(t)} \varphi \, \vec{q}_b \cdot \hat{n} \, dS_n \quad , \quad \forall \vec{x} \in V(t)$$

$$T = T_b \qquad \forall \vec{x} \in S_{D,T}$$

Discretization:

$$T = \mathbf{N}\boldsymbol{\theta}$$

using the same shape functions as $\vec{v}$ and p.

Thermo-mechanical coupling – Discrete form

Discrete version of the energy conservation equations:

$$\mathbf{M}_{\rho c_V} \frac{d}{dt}\boldsymbol{\theta} = -\mathbf{L}_k \boldsymbol{\theta} + \mathbf{s}_{\text{ext}}$$

with:

$$\mathbf{M}_{\rho c_V} = \int_{\Omega(t)} \rho c_V \mathbf{N}^{\mathsf{T}} \mathbf{N} \, d\Omega \qquad \mathbf{L}_k = \int_{\Omega(t)} k \nabla \mathbf{N}^{\mathsf{T}} \nabla \mathbf{N} \, d\Omega$$

$$\mathbf{s}_{\text{ext}} = \int_{\Gamma(t)} \mathbf{N}^{\mathsf{T}} \vec{q}_b \cdot \hat{n} \, d\Gamma$$

and:

$$\boldsymbol{\theta} = \begin{bmatrix} \theta_1 & \theta_2 & \theta_3 & \theta_4 \end{bmatrix}$$

Thermo-mechanical coupling – Solution strategy

In the implicit solver:

$$\left(\frac{1}{\Delta t}\mathbf{M}_{\rho c_V}^{n+1} + \mathbf{L}_k^{n+1}\right)\boldsymbol{\theta}^{n+1} = \mathbf{s}_{\text{ext}}^{n+1} + \frac{1}{\Delta t}\mathbf{M}_{\rho c_V}^{n+1}\boldsymbol{\theta}^{n},$$

in the explicit solver:

$$\boldsymbol{\theta}^{n+1} = (\mathbf{M}_{\rho c_V}^{n})^{-1}((\mathbf{M}_{\rho c_V}^{n}\boldsymbol{\theta}^{n} - \mathbf{L}_k^{n})\boldsymbol{\theta}^{n} + \mathbf{s}_{\text{ext}}^{n}).$$

Thermo-mechanical coupling – Solution strategy

Currently, for each time step, the energy equation is always solved first, and then the momentum/continuity equations are solved.

Loop over time steps:

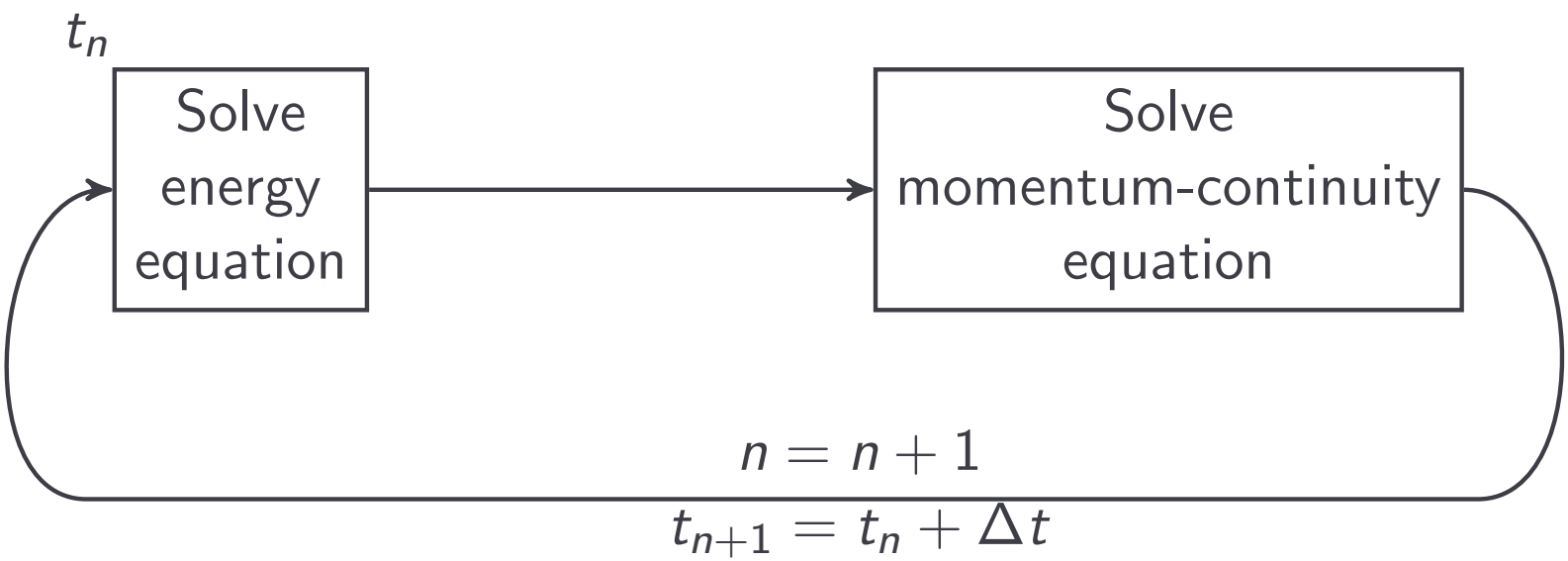

Validation

From literature

Front view orthogonal to scanning direction:

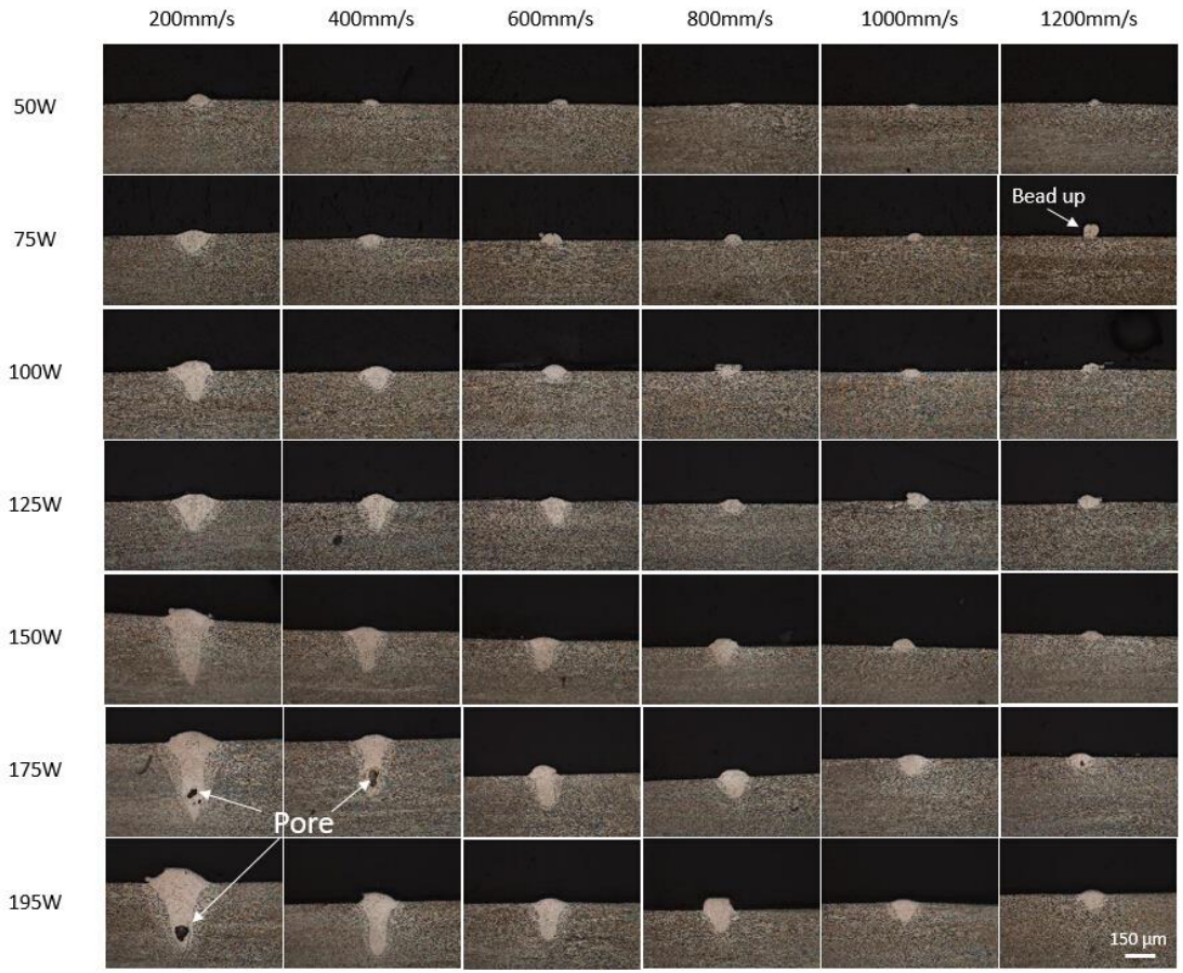

Melt pool profile of single beads (powder case, Ti-6Al-4V); from Gong 2014.

Stay at CEMEF (Summer 2022)

Verification: comparison with existing solver and with experiments (no vaporization, no spattering!).

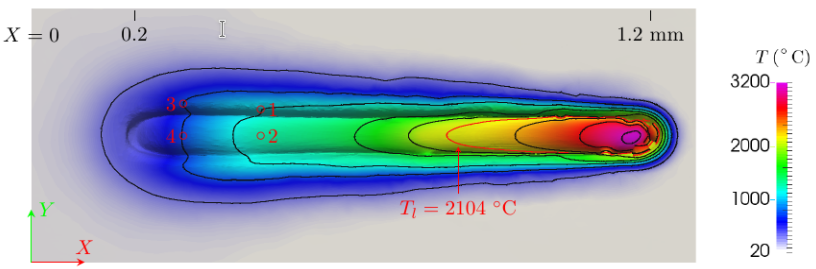

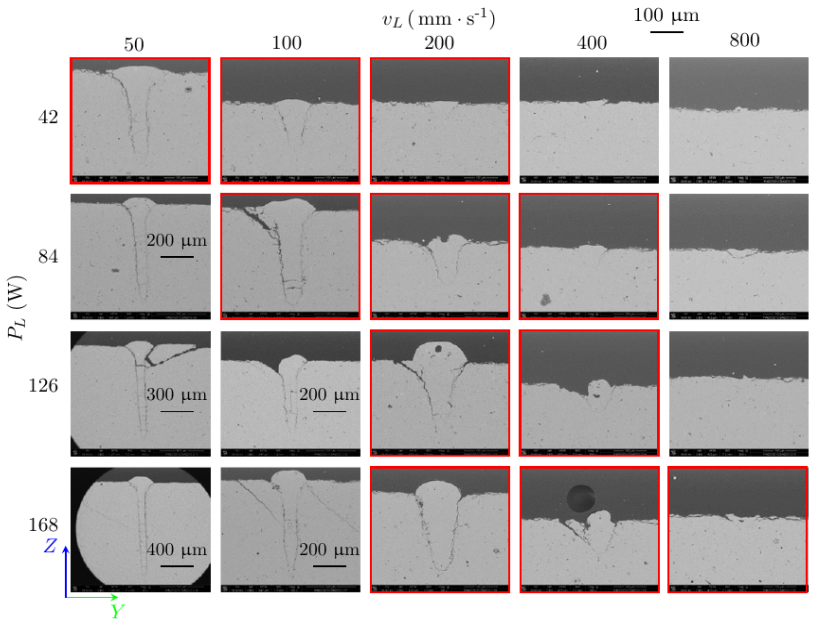

From Chen 2018.

N.B.: if health situation allows it

Project LongLifeAM

WALInnov - Walloon Region - 01/01/2019 to 31/12/2022.

Collaboration: J.-P. Ponthot (PI; MN2L, ULiège), A. Simard (UCL), A.-M. Habraken (MSM, ULiège) and A. Mertens (MMS, ULiège).

Fatigue properties of SLM-AlSi10Mg components $\rightarrow$ many experimental results generated during the project.

Project AlFeWeld

WALInnov - Walloon Region - 01/06/2019 to 31/05/2023.

Collaboration: A. Simard (PI; UCL), P. Jacques (UCL) and J.-P. Ponthot (MN2L, ULiège).

Improvements of Friction Melt Bonding (welding process for dissimilar materials):

- existence of a melt pool,
- many experimental results generated during the project,
- no keyhole, no free surface (trapped molten pool)!.

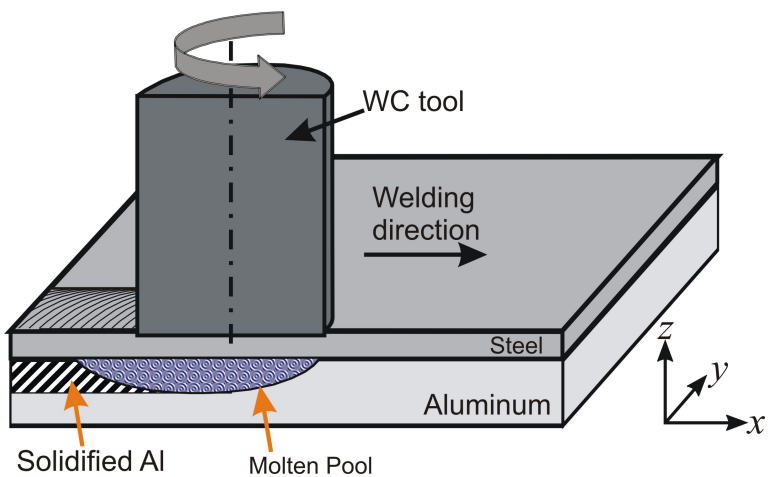

Principle of FMB

Collaboration with Pr. A. Mertens and A.-M. Habraken

Collaboration: A. Mertens (MMS, Uliège), A.-M. Habraken (ULiège), J.-P. Ponthot (MN2L, Uliège): LonglifeAM, ARC (under evaluation).

Acquisition of SLM machine.

- Preheating plate;
- Al, stainless steel, Ni-Cr, Co-Cr alloys;
- microstructural characterization:
  - defects, keyholes,
  - melt pool size,
  - phases identification (optical and electron beam microscope);
- IR camera, thermocouples.

LM-Innovations – Alpha 140

Collaboration with Pr. A. Mertens and A.-M. Habraken

Complementarity: numerical and experimental.

$\Rightarrow$ day to day collaboration.

$\Rightarrow$ approach based on iterative mutual improvements.

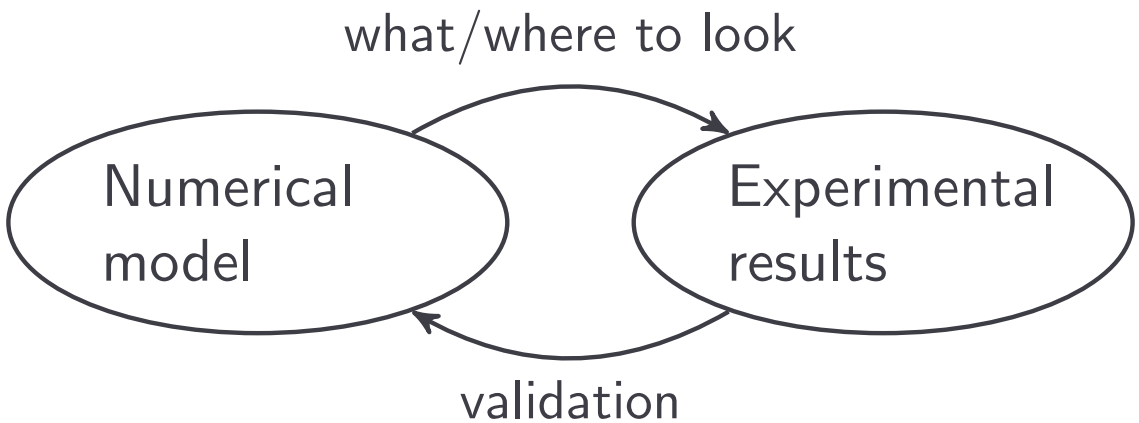

Curvature computation in 3D

The basics: the platelet points

This section is based on Hamman B., *Curvature Approximation for Triangulated Surfaces*, Geometric Modelling, Springer Vienna, 1993. All figures have been generated using the *Geogebra 5* software.

To compute the curvature at one node of the free surface, discretized by triangular facets, we first have to identify the neighbours of that node on the free surface (the platelet points).

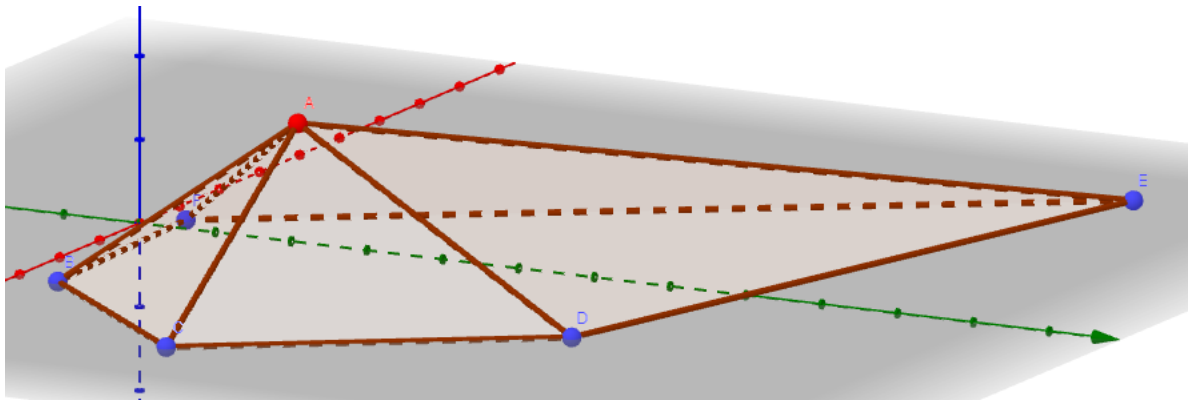

The platelet points of node A.

Node normal

Then, the normal of each triangle adjacent to the node is computed, and the normal of the free surface at the node is computed as:

$$\hat{n}_A = \frac{\sum_{i=0}^{N_{facets}} \alpha_i \hat{n}_i}{\| \sum_{i=0}^{N_{facets}} \alpha_i \hat{n}_i \|}$$

where α_i is the angle made by the facet i at the node.

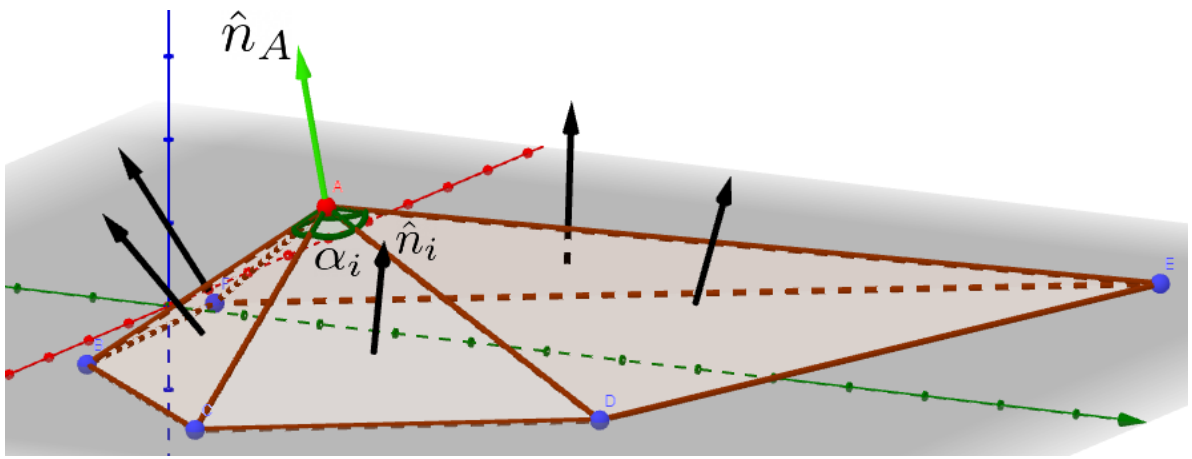

Computation of the free surface normal at node A.

Guiding plane

The plane passing through the node and having normal $\hat{n}$ is computed.

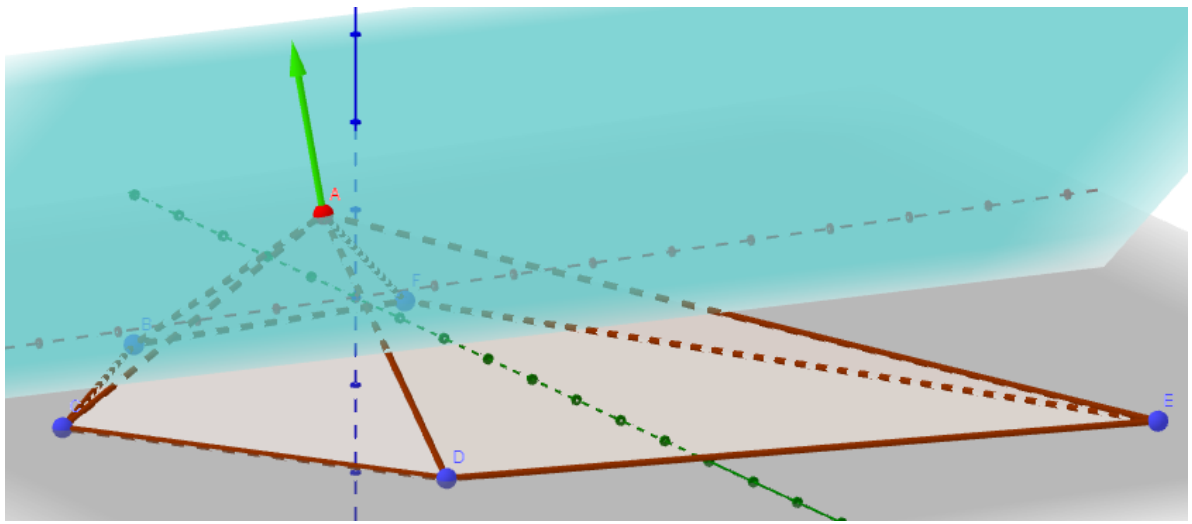

The guiding plane.

Projection of platelet points

The points constituting the platelet are projected onto the guiding plane to obtain their projection as well as their distance from the plane (d_i)

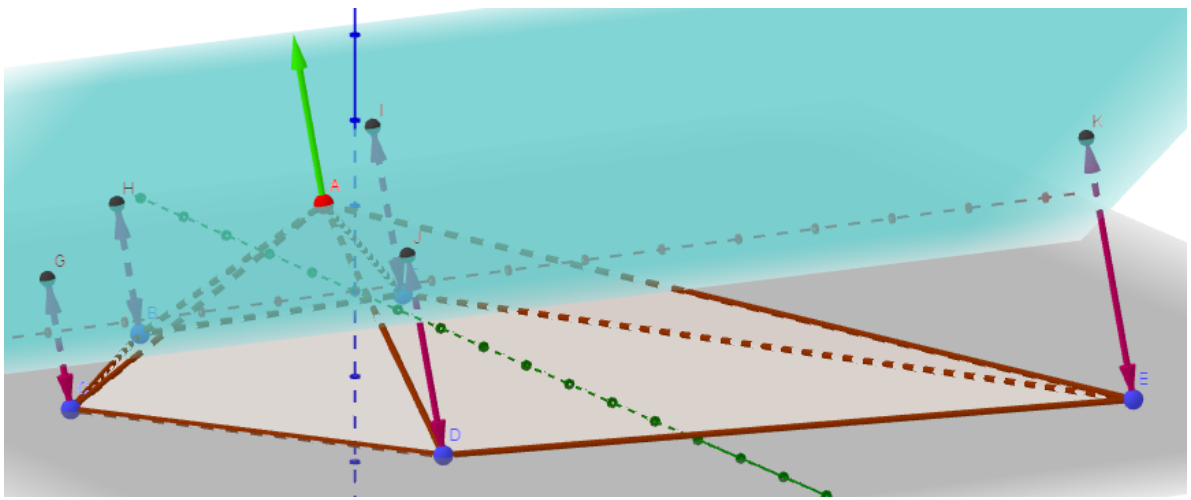

Projection of the platelet points on the guiding plane.

Guiding plane director vectors

Two director vectors of the guiding plane are computed:

$$\hat{b}_1 = \begin{cases} (-(n_y + n_z)/n_x, 1, 1)^\mathsf{T} & n_x \neq 0 \\ (1, -(n_x + n_z)/n_y, 1)^\mathsf{T} & n_y \neq 0 \\ (1, 1, -(n_x + n_y)/n_z)^\mathsf{T} & n_z \neq 0 \end{cases}$$

$$\hat{b}_2 = \hat{n} \times \hat{b}_1$$

With the plane normal, they will form a local basis $(\hat{b}_1, \hat{b}_2, \hat{n})$ with associated coordinates (u, v, d).

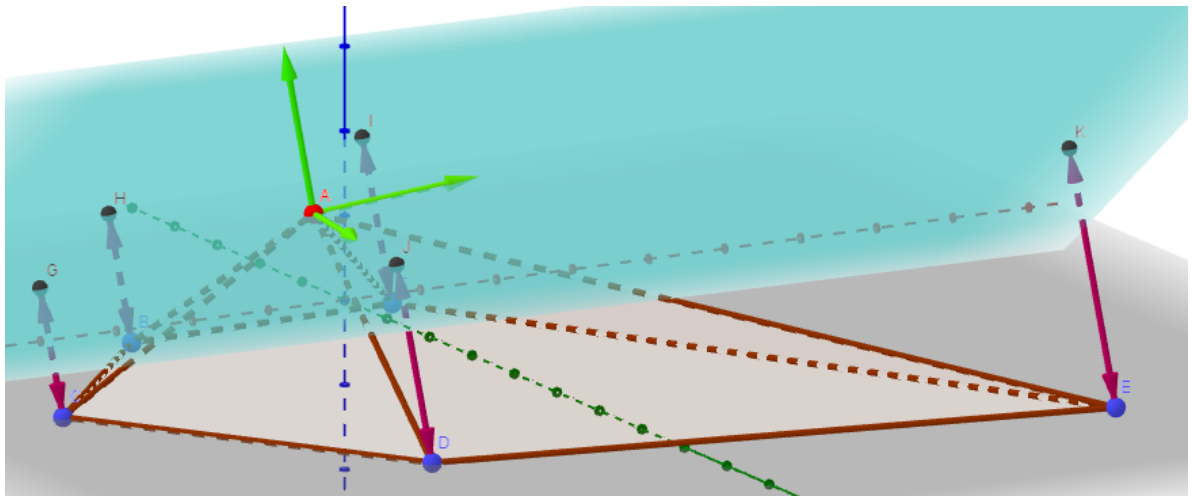

Guiding plane local basis.

Coordinate of the platelet points in the local basis

A polynomial of the form (auscultating paraboloid):

$$f(u, v) = 0.5(au^2 + 2buv + cv^2)$$

is fitted in the guiding plane local basis (u and v the coordinate in the plane) using a least-square method (a, b and c the coefficient to determine):

$$\mathbf{U} = 0.5 \begin{pmatrix} u_1^2 & 2u_1v_1 & v_1^2 \\ \vdots & \vdots & \vdots \\ u_n^2 & 2u_nv_n & v_n^2 \end{pmatrix} \quad \mathbf{d} = \begin{pmatrix} d_1 \\ \vdots \\ d_n \end{pmatrix} \quad \Rightarrow \mathbf{U}^\mathsf{T}\mathbf{U} \begin{pmatrix} a \\ b \\ c \end{pmatrix} = \mathbf{U}^\mathsf{T}\mathbf{d}$$

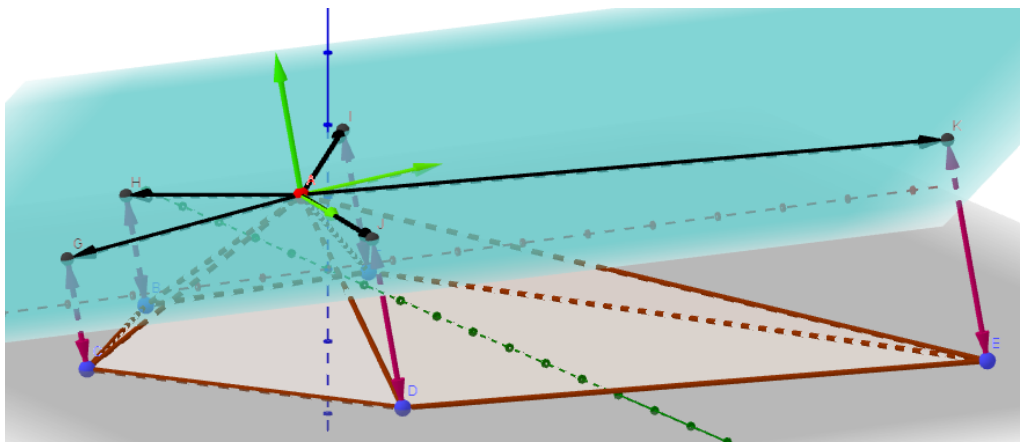

Platelet points in the local basis

Curvature computation

The two principal curvatures are given by the two real roots of:

$$\kappa^2 - (a + c)\kappa + ac - b^2 = 0$$

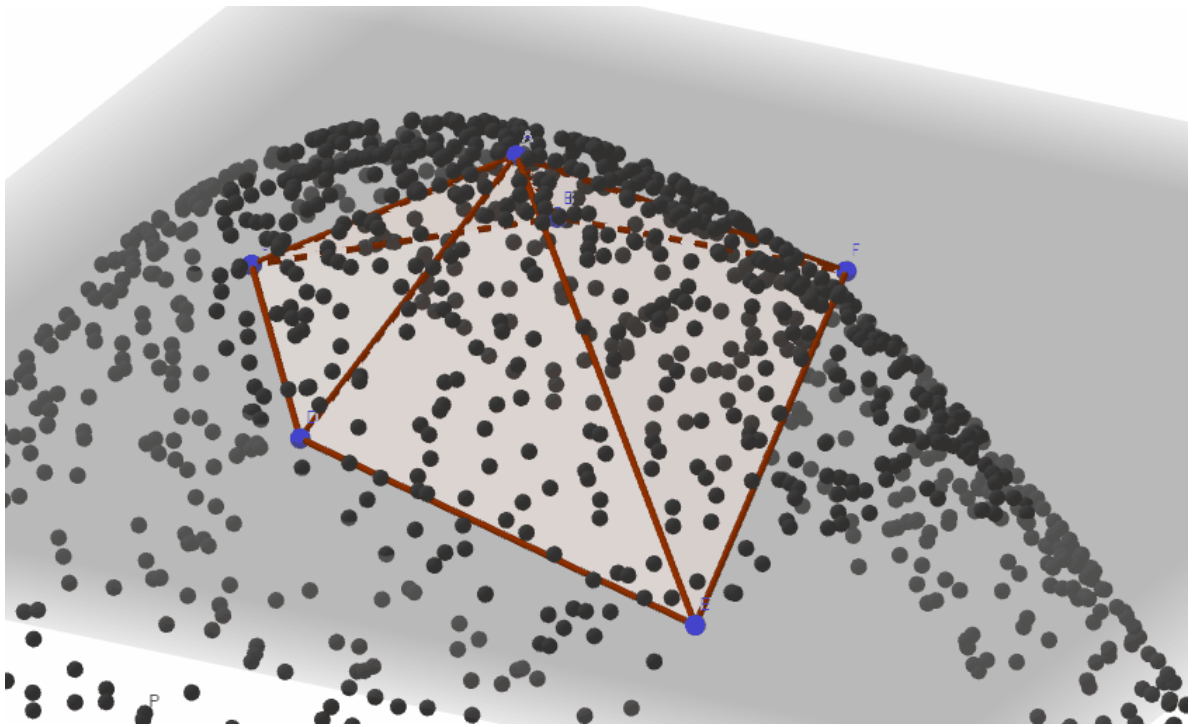

Auscultating paraboloid visualization.

Curvature computation

The two principal curvatures are given by the two real roots of:

$$\kappa^2 - (a + c)\kappa + ac - b^2 = 0$$

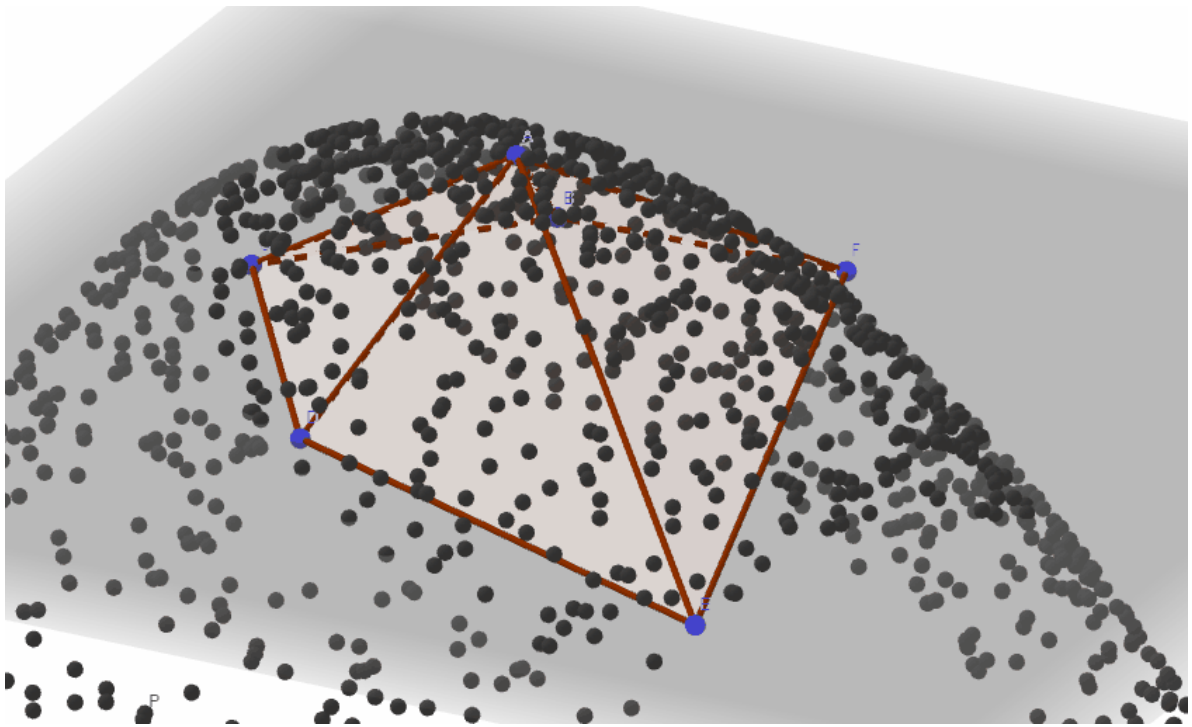

Auscultating paraboloid visualization.

Remeshing in the PFEM

Delaunay triangulation

2D definition: triangulation with no other points inside the circum-circle of one of the triangle.

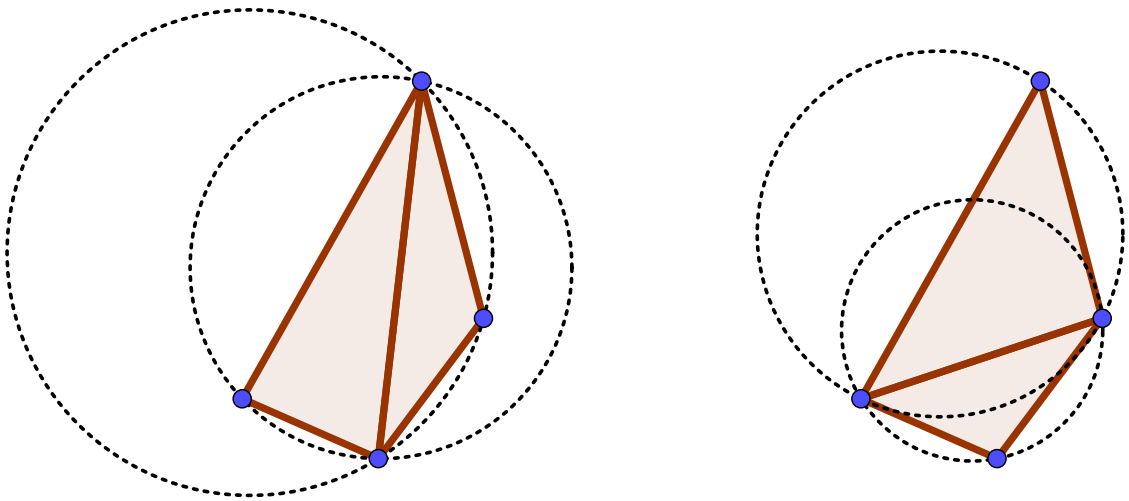

Two triangulations of four points, Delaunay on the right.

3D definition: same with circumsphere.

Delaunay triangulation

Delaunay triangulation will deliver the convex hull of the cloud of points.

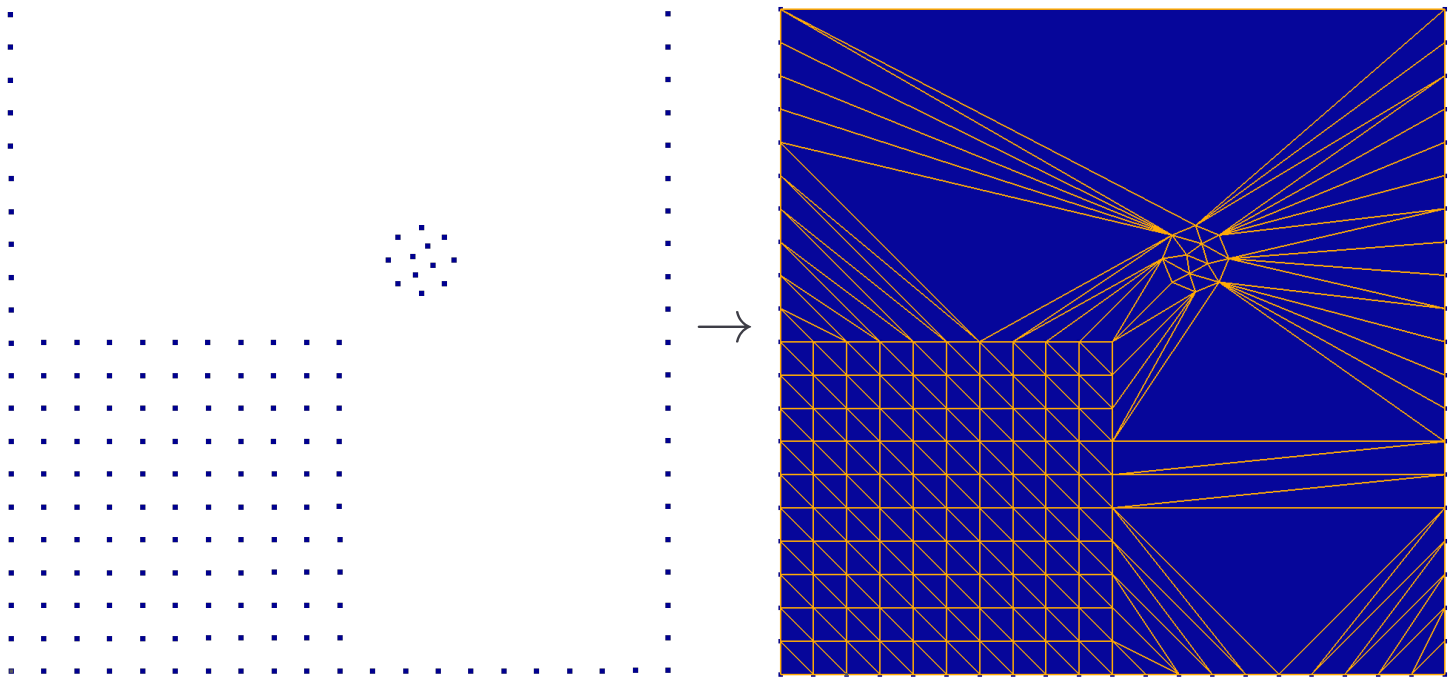

Example of Delaunay triangulation on a cloud of nodes, from Février's master thesis.

To eliminate spurious triangle and determine free surface $\rightarrow$ α-shape algorithm.

Alpha-shape algorithm

Goal: automatically determine external surfaces.
Definition: "A simplex is said α-exposed if there is an open disk/open sphere of radius $\sqrt{\alpha}$ through the vertices of the simplex that does not contain any other point of the set"

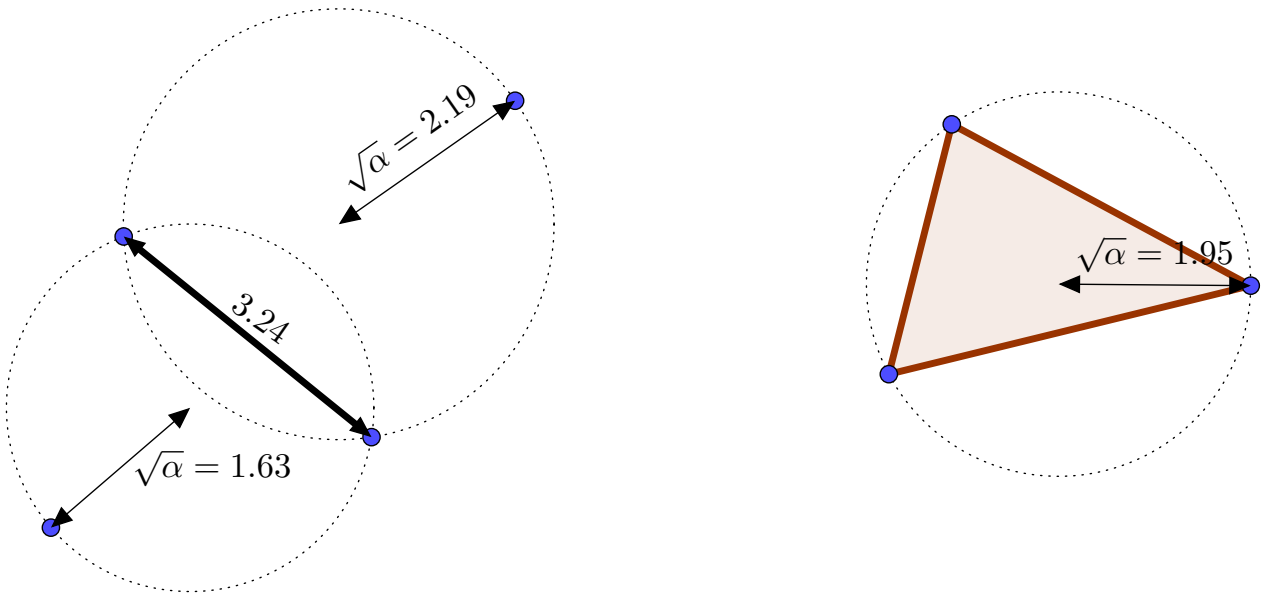

Minimum and maximum α value of a 1-simplex (on the left) and a 2-simplex (on the right) for which they remains α-exposed in 2D, from Février's master thesis.

Alpha-shape algorithm

Alpha-shape algorithm applied to the square and disk in a box triangulation.

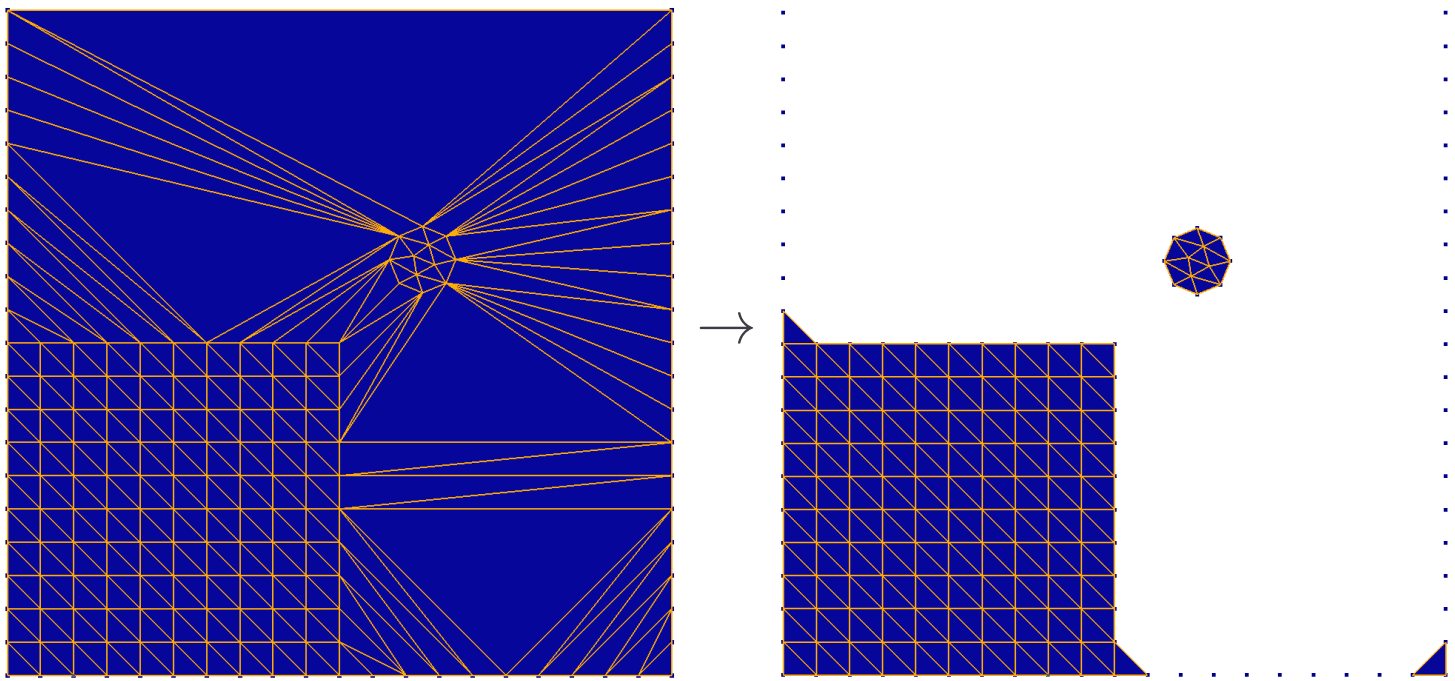

Example of alpha-shape algorithm ($\alpha = 1.25$), from Février's master thesis.